JGR Solid Earth

RESEARCH ARTICLE
10.1029/2022JB025379

Key Points:

- Source of enriched MORB (E-MORB) from the Central Indian Ridge (12°–17°S) is constrained by Sr-Nd-Pb isotope and trace element geochemistry
- The E-MORB source between 14° and 16°S is related to three components: a depleted mantle, Réunion Plume (RP), and continental components
- Variable proportions of continental components mixed with the RP may account for the MORB geochemistry between 14° and 20°S

Supporting Information:

Supporting Information may be found in the online version of this article.

Correspondence to:

C. Vincent,
clementvincent@snu.ac.kr

Citation:

Vincent, C., Park, J.-W., Lee, S.-M., Kim, J., Lee, M.-J., & Révillon, S. (2022). Heterogeneous fossil Réunion plume component in the source region of enriched MORB along the Central Indian Ridge between 12° and 17°S. *Journal of Geophysical Research: Solid Earth*, *127*, e2022JB025379. https://doi.org/10.1029/2022JB025379

Received 16 AUG 2022
Accepted 24 NOV 2022

Author Contributions:

Formal analysis: Clément Vincent, Sang-Mook Lee, Mi-Jung Lee, Sidonie Révillon
Funding acquisition: Jung-Woo Park, Sang-Mook Lee
Supervision: Jung-Woo Park, Sang-Mook Lee, Jonguk Kim, Sidonie Révillon
Validation: Jung-Woo Park, Mi-Jung Lee, Sidonie Révillon
Writing – original draft: Clément Vincent
Writing – review & editing: Clément Vincent, Jung-Woo Park, Sang-Mook Lee, Jonguk Kim, Sidonie Révillon

Heterogeneous Fossil Réunion Plume Component in the Source Region of Enriched MORB Along the Central Indian Ridge Between 12° and 17°S

Clément Vincent[1], Jung-Woo Park[1,2], Sang-Mook Lee[1], Jonguk Kim[3], Mi-Jung Lee[4], and Sidonie Révillon[5]

[1]School of Earth and Environmental Sciences, Seoul National University, Seoul, South Korea, [2]Research Institute of Oceanography, Seoul National University, Seoul, South Korea, [3]Deep-Sea and Seabed Mineral Resources Research Center, Korea Institute of Ocean Science & Technology, Busan, South Korea, [4]Division of Earth Sciences, Korea Polar Research Institute, Incheon, South Korea, [5]SEDISOR/Geo-Ocean University Brest-CNRS-IFREMERUMR 6538, Institut Universitaire Européen de la Mer IUEM, Brest, France

Abstract Mid-ocean ridge basalts (MORB) from the Central Indian Ridge (CIR) between 12° and 17°S show a wide range of geochemical and isotopic variations. Particularly, MORB from a segment between 14° and 15°S are more enriched in incompatible trace elements with more radiogenic Sr and Pb isotope and unradiogenic Nd isotope values than the lavas between 15° and 16°S with geochemical features of normal MORB. However, the causes for the enrichment between 14° and 15°S are poorly constrained. In this study, we re-examined the CIR MORB from 12° to 17°S with new geochemical data obtained based on high spatial resolution sampling to better understand the nature of the enriched mantle source. Our new geochemical data show that the MORB between 14° and 15°S, with maximum values for $(La/Sm)_N = 1.95$, $^{87}Sr/^{86}Sr = 0.703526$ and $^{206}Pb/^{204}Pb = 18.7558$, are more enriched than those from the southern segments (16° to 20°S) known to be influenced by the Réunion mantle component. The new trace element and isotopic compositions of MORB suggest that three mantle end-members are required to explain the geochemical variations shown between 14° and 16°S: the depleted Indian-type MORB mantle, Réunion Plume (RP), and Seychelles/Madagascar-like continental crust components. Moreover, our mixing model suggests that the differences in enriched MORB signature from 14° to 20°S are due to variable proportions of continental material previously mixed with the RP. Our study implies that a continental component interacted with the plume into the asthenosphere, possibly beneath Madagascar or below Mauritius Island and the Mascarene plateau.

Plain Language Summary The basaltic lavas erupting on the mid-ocean ridges are considered a window to understand the geochemical features of the upper mantle because they are produced by partial melting of the underlying mantle. The mid-ocean ridge basalts (MORB) from the Central Indian Ridge (CIR) between 12° and 17°S show a wide range of geochemical and isotopic variations. Particularly, the MORB from the segment between 14° and 15°S have higher trace element contents with more radiogenic Sr and Pb isotopes and unradiogenic Nd isotopes than those from the neighboring ridges. We investigated the mantle source of the E-MORB using our new geochemical data of basaltic lava samples collected with high spatial resolution along the ridge between 12° and 17°S and showed that the enriched lavas between 14° and 15°S are not only linked to the Réunion mantle plume, but also to a continental crust component that contaminated the Réunion mantle plume. Moreover, our new results enlarge the isotopic range of the Réunion mantle plume and show the complexity and heterogeneity of the upper mantle underlying the CIR.

1. Introduction

The geochemical and isotope characteristics of mid-ocean ridge basalts (MORB) sampled along mid-ocean ridges axis provide direct information on the composition of the underlying shallow mantle. The normal MORB (N-MORB) signature represents the depleted nature of the ambient upper mantle. However, enriched MORB (E-MORB) sampled reservoirs with variably enriched compositions compared to the depleted ambient upper mantle. The E-MORB mantle source has been traditionally explained by the influence of mantle plumes bringing enriched components that influence the melting regime or interact directly with portions of the oceanic crust (Hart et al., 1973; Ito et al., 2003; Schilling, 1973, 1985). Metasomatized lithospheric mantle (e.g., Donnelly et al., 2004; Galer & O'Nions, 1986) or recycled oceanic crust (Hémond et al., 2006; Hofmann, 1997; Hofmann

& White, 1982; Ulrich et al., 2012) are other potential enriched sources involved in E-MORB genesis when geochemical anomalies cannot be linked with any local hotspot or plume.

MORB geochemical variations from the Central Indian Ridge (CIR), particularly along the segments adjacent to the Marie Celeste Fracture Zone (MCFZ), have been investigated in order to understand E-MORB mantle sources and the exact relationship between the Réunion Plume (RP) and CIR. Previous studies have shown that the CIR crossed the RP location at about 34 Ma (Duncan, 1990; O'Neill et al., 2003; Torsvik et al., 2013). The ridge then progressively moved away to reach its current position, with the Réunion hotspot being located more than 1,000 km from the ridge axis (Füri et al., 2011; Mahoney et al., 1989; Nauret et al., 2006). Throughout the migration of the CIR to the northeast, the RP continued its interaction with segments of the CIR. Previous studies showed an enriched geochemical signature in the southern part of the Rodrigues segment of the CIR (from 17° to 21°S, Figure 1) that may be associated with lateral flow from the RP (Füri et al., 2011; Nauret et al., 2006). Furthermore, a recent seismologic study (Barruol et al., 2019) shows the presence of a shallow asthenospheric flow connecting the Réunion hotspot to the Rodrigues segment, confirming the current connection between these two magmatic systems.

Although MORB from the northern portion of the Rodrigues segment (Figure 1b) also display an enriched signature, Nauret et al. (2006) showed that this enriched signature differs from the one along the southern portion and the recent lava of the Piton de la Fournaise volcano, the actual surface expression of the Réunion hotspot. They claimed that the enriched anomaly in the north of the Rodrigues segment is not due to the RP but to a discrete enriched mantle source, possibly an upper mantle enriched by a low-degree melt metasomatic process (Donnelly et al., 2004) or from ancient basaltic oceanic islands recycled by subduction. Later, Füri et al. (2011) proposed that the MORB enrichment anomaly in the northern part of the Rodrigues segment could either originate from a metasomatized mantle or a fossil Réunion mantle component since the RP crossed the CIR at ~34 Ma. Alternatively, Ulrich et al. (2012) argued that the enrichment can be the result of recycled oceanic-island basalt (OIB) by ancient subduction, which formed upper mantle heterogeneity beneath the ridge. The ridge portions north of the Rodrigues segment (Segment 5 and 6 in Figure 1c) also show an EM2-like enriched geochemical signature that was attributed to a fossil Réunion mantle component by Kim et al. (2017), which is consistent with the argument suggested by Füri et al. (2011) for the north Rodrigues segment.

To sum up, the studies conducted along the CIR are not unanimous on the origin of the E-MORB source along segments 5, 6 and the northern portion of the Rodrigues segment. It is not clear whether these enrichments result from an enriched source related to a fossil component from the past influence of the RP or the involvement of heterogeneities unrelated to the RP.

In order to better constrain the CIR enriched mantle source between 12° and 17°S (north of the MCFZ; Figure 1c) and the possible extent in the shallow mantle of the RP component, a series of new analyses of major and trace elements as well as Sr, Nd, and Pb isotopic compositions of MORB from the segments 5 and 6 (Figure 1c) were conducted. Our new geochemical data provide much higher spatial resolution than previous studies, allowing a better localization and delimitation of the enriched portions along the ridge axis, particularly along segment 5.

The results show that the source of E-MORB along segment 5 is distinguished from the RP. The enriched signature along segment 5 requires the presence of at least three different components in the melting regime. Based on the E-MORB signature and a two-step binary mixing model, we propose that segment 5 and most certainly segment 6 and the Rodrigues segment involve the depleted CIR MORB mantle and the fossil RP component that was previously contaminated in different proportions by a continental component (i.e., a Seychelles/Madagascar component).

2. Geological Setting and Background

The CIR (Figure 1) lies north of the Rodrigues Triple Junction (at 25°S, 70°E) and south of 3°S. It is a slow to intermediate spreading mid-ocean ridge (DeMets et al., 1990, 1994, 2010; Münch et al., 1999; Pak et al., 2017), separating the African and Capricorn plates. In the last decade, new geochemical data, as well as magnetic and bathymetric data, have been collected along the branch of the CIR north of the MCFZ, including three segments between 12° and 17°S, the segments 4, 5, and 6 from north to south (nomenclature after Pak et al., 2017, Figure 1).

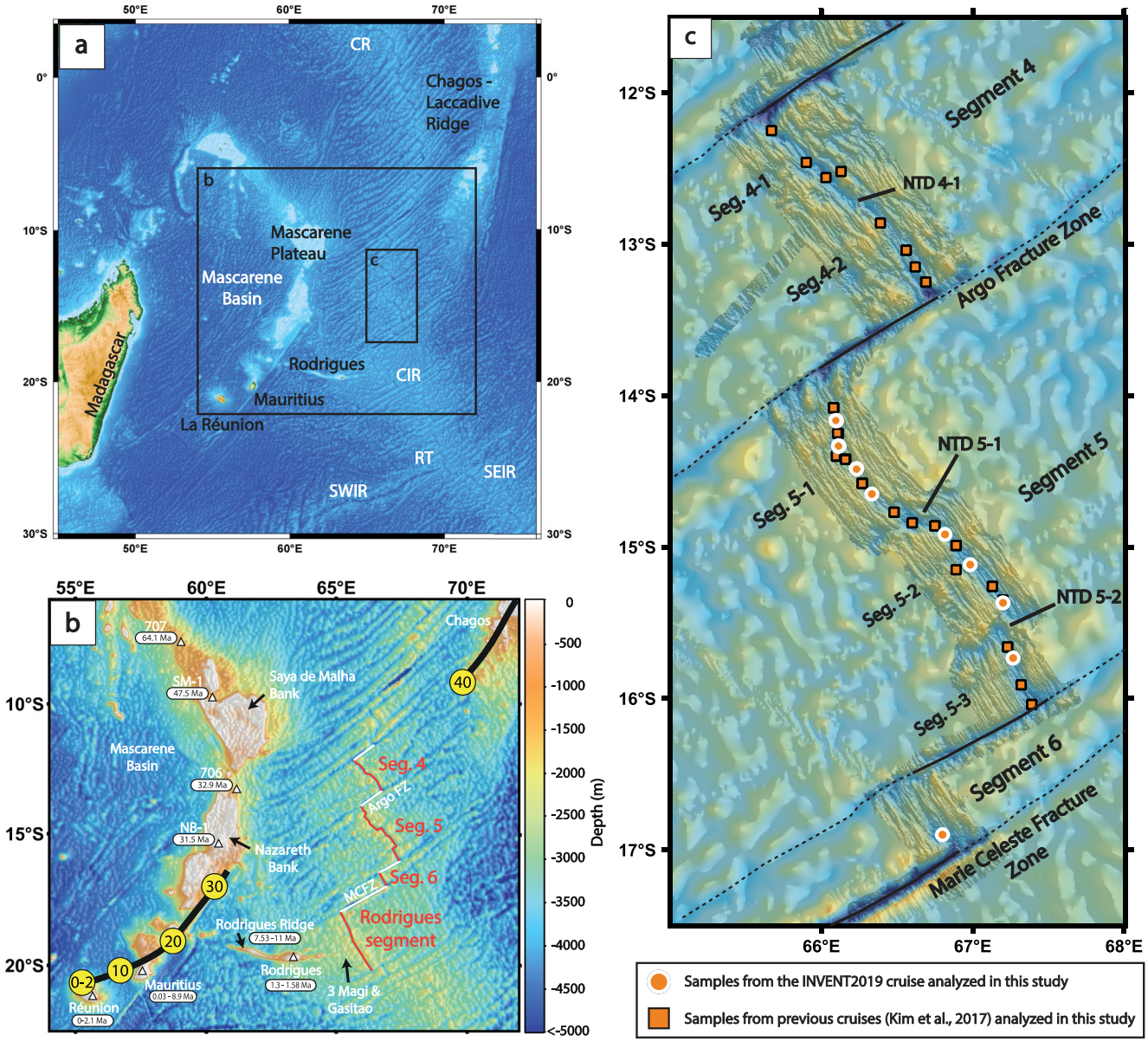

Figure 1. (a) Geological setting map of the Central Indian Ridge (CIR) region modified from ETOPO1 (Amante & Eakins, 2009). (b) Bathymetric map of the middle part of the CIR and the calculated tracks of the Réunion hot spot based on plate model by O'Neill et al. (2003) with circled yellow numbers representing age in Ma. The triangles denote dated sites from ODP Legs 115 (holes 706, 707, and 715) and industry wells (SM-1 and NB-1) (age from Duncan, 1990). The age range of the Rodrigues Ridge and Rodrigues island are from Mellor (1998) and McDougall et al. (1965) respectively. (c) Bathymetric map of the segment 4, 5, and 6 and their segments (e.g., Seg 4-1) with the sample locations analyzed in this study. The orange and white dots represent the samples newly dredged during the INVENT2019 cruise and the orange and black squares are the samples dredged during previous cruises (Kim et al., 2017). The black and the dashed black lines denote transform fault and fracture zone, respectively. The identified second-order non-transform discontinuities from Pak et al. (2017) are indicated by non-transform discontinuities (NTDs) with numbers (e.g., NTD 5-1). RT: Rodriguez Triple Junction; SWIR: Southwest Indian Ridge; SEIR: Southeast Indian Ridge; CR: Carlsberg Ridge.

These three segments have lengths of 175 km (segment 4), 281 km (segment 5), and 63 km (segment 6), forming a 518-km-long portion of the CIR (Figure 1). These segments are offset >30 km by well-defined dextral transform faults (TF) and divided into a few subsegments that are offset by second-order (offset <30 km) non-transform discontinuities (NTDs) (Pak et al., 2017). The segment 4 is divided into two subsegments, segment 4-1 and segment 4-2, by the NTD 4-1 at 12.72°S (Figure 1c). On the other hand, the segment 5 is divided into three subsegments (segments 5-1, 5-2, and 5-3) by NTD 5-1 and NTD 5-2 at 14.85° and 15.5°S, respectively. Oceanic core complexes were observed at the corners of the segments, occurring in proximity to TFs and NTDs (Pak et al., 2017).

Réunion Island, and its active Piton de la Fournaise volcano, mark the surface expression and the current position of the Réunion hotspot, located approximately 1,100 km to the east of the CIR axis (Figure 1) (Gillot & Nativel, 1989; Richards et al., 1989). The hotspot can be tracked from the Deccan Traps in India to Réunion Island, which represents 65.5 Myr of volcanic activity (Courtillot et al., 1986; Richards et al., 1989; Torsvik et al., 2013). After forming the Deccan Trap flood basalts, the RP formed the Chagos–Maldives–Laccadive Ridge, the Mascarene Plateau (McKenzie & Sclater, 1971), and the Mascarene Islands, which comprises the islands of Réunion, Mauritius, and Rodrigues (Duncan, 1990; Duncan et al., 1989) (Figure 1). The middle part of the CIR can be linked to the trajectory of past Réunion hotspot activity from the southern end of the Chagos-Laccadive Ridge. Accordingly, the Mascarene Plateau and the Chagos-Laccadive Ridge are separated by the CIR spreading at segments 4, 5 and 6, which are the focus of this study.

3. Sampling and Analytical Methods

Submarine pillow basalts were collected by dredging during the INVENT2019 expedition by R/V ISABU in 2019 along the south of the CIR (between 14° and 17°S). A single dredge was done successfully along the spreading axis from segment 6, and eight dredges were conducted along segment 5. Variable amounts of fresh glasses were collected from all the dredges. In addition to these new samples, 24 samples of fresh basaltic glasses from previous cruises of the R/V Onnuri (part of the KODOS program; Kim et al., 2017) were selected for further Sr, Nd, and Pb isotope analysis. A total of 10 samples were selected from segment 4 and 14 samples from segment 5.

Major and trace element compositions of 25 new samples (Table S1 in Supporting Information S1) from the 2019 expedition (nine dredge locations with an average of three samples per dredge) were determined on submarine glass fragments in carbon-coated epoxy mounts. Major element contents were determined by a JEOL JXA-8530F field-emission electron probe microanalyzer (FE-EPMA) at the National Center for Inter-university Research Facilities at Seoul National University. The analysis was conducted with an accelerating voltage of 15 kV, a current of 20 nA, and a beam diameter of 3 μm. Natural minerals and synthetic oxides were used as calibration standards. The reference standard Smithsonian basalt glass (VG-2) was analyzed with each set of unknown samples to monitor instrumental drift, accuracy, and precision. Analytical uncertainties are the 2σ analytical error, obtained from the replicate measurements ($n = 20$) of the VG-2 glass standard (see Table S1 in Supporting Information S1). Except for K_2O having concentrations close to the detection limits, all microprobe data for those major elements are accurate, with analytical uncertainties of <3%. Minor and trace element contents were measured by laser-ablation inductively coupled plasma mass spectrometer (LA-ICP-MS) using an Agilent 7,700 quadrupole ICP-MS combined with an ESI New Wave 193 nm excimer laser at the Deep-Sea Mineral Resources Research Center, Korea Institute of Ocean Science and Technology (KIOST). LA-ICP-MS analysis was operated with laser pulse rates of 10 Hz, energy density of 5 J/cm^2, and spot sizes of 150 μm. Each analysis is composed of 60 s of data acquisition, with background count rates measured for 30 s prior to analysis. The NIST 612 was analyzed with the set of samples as a primary standard for trace elements. Data reduction was undertaken using the method described in Park et al. (2012), with ^{43}Ca contents measured by electron probe microanalyze as the internal standard. Micro inclusions were excluded based on the time-resolved spectra. The USGS glass BCR-2G and BHVO-2G were analyzed regularly ($n = 7$) as unknown samples for externally quantifying the precision and accuracy of the analysis. The trace element data are accurate within ±5% differences except for Pb of BHVO-2G (16%), which may be due to the low Pb concentrations (1.83–2.05 ppm).

Thirty-five samples were analyzed for Sr, Nd, and Pb isotopes in three different laboratories. The fresh basalt samples were crushed and sonicated in distilled water until no turbidity was observed before being dried. The glass fragments were carefully hand-picked using a binocular microscope to exclude those showing signs of alteration. In order to remove carbonate, 31 samples (see Table 1 and Table S2 in Supporting Information S1) were leached in 2M HCl for 10–20 min, depending on their conditions, on a hot plate at 60°C. Four samples (IR090301, IR10022701, IR10022901 and IR10021501) did not undergo any prior HCl leaching in order to confirm their anomalous Sr and Nd isotopes ratios previously reported by Kim et al. (2017) and the result is presented and discussed in Section 4.2. The leached samples were then powdered in an agate mortar for Sr, Nd, and Pb isotope analyses.

Strontium and Nd isotope analyses of 19 samples were performed at KBSI (Korea Basic Science Institute) using a multi-collector thermal ionization mass spectrometry (TIMS; Isoprobe-T). Four samples (IR090301, IR10022701, IR10022901, and IR10021501), previously reported by Kim et al. (2017), were re-analyzed by SEDISOR in Brest

Table 1
Sr, Nd, and Pb Isotopic Compositions in Mid-Ocean Ridge Basalts Glasses From the Central Indian Ridge Segments Between 12° and 17°S (Segment 4, 5 and 6)

Sample	Segment	Latitude (°S)	Longitude (°E)	Depth (m)	$^{87}Sr/^{86}Sr$	$^{143}Nd/^{144}Nd$	$^{206}Pb/^{204}Pb$	$^{207}Pb/^{204}Pb$	$^{208}Pb/^{204}Pb$
IR090703 g*	Seg. 4	12.25	65.67	4,101	0.702847 ± 8	0.513103 ± 5			
IR090401 g*	Seg. 4	12.46	65.90	3,784	0.702805 ± 8	0.513078 ± 4			
IR110307*	Seg. 4	12.52	66.13	3,031	0.702846 ± 9	0.513098 ± 4			
IR090301[3]	Seg. 4	12.56	66.03	4,371	0.702968 ± 6	0.513032 ± 9			
IR110213-3*	Seg. 4	12.86	66.39	2970	0.702979 ± 9	0.513091 ± 4			
IR100229013	Seg. 4	13.04	66.56	3,324	0.702977 ± 6	0.513084 ± 8			
IR10022902*	Seg. 4	13.04	66.56	3,324	0.702944 ± 11	0.513090 ± 5			
IR110215-1_u*	Seg. 4	13.15	66.62	3,524	0.702917 ± 8	0.513110 ± 5			
IR100227013	Seg. 4	13.25	66.69	3,929	0.702887 ± 6	0.513102 ± 9			
IR10022702*	Seg. 4	13.25	66.69	3,929	0.702852 ± 9	0.513015 ± 13			
IR10022401*	Seg. 5	14.08	66.08	3,253	0.703121 ± 10	0.513018 ± 3			
IR10022401[2]					0.703128 ± 6	0.513022 ± 11	18.4820 ± 17	15.5303 ± 16	38.4560 ± 50
RD1911-05 g[2]	Seg. 5	14.17	66.10	3,273	0.703036 ± 7		18.3936 ± 22	15.5279 ± 21	38.3983 ± 64
IR10022301*	Seg. 5	14.25	66.11	3,868	0.703232 ± 9	0.513004 ± 4			
IR10022301[2]					0.703190 ± 7	0.513028 ± 15	18.5095 ± 18	15.5536 ± 16	38.5827 ± 51
RD1910-02 g[2]	Seg. 5	14.33	66.12	3,502	0.703392 ± 9	0.512972 ± 7	18.6510 ± 14	15.5800 ± 13	38.8363 ± 41
IR110231-1[2]	Seg. 5	14.40	66.10	3,133	0.703497 ± 8	0.512974 ± 15	18.6161 ± 19	15.5763 ± 18	38.7831 ± 57
IR10022201*	Seg. 5	14.42	66.16	3,492	0.703139 ± 8	0.513017 ± 4			
IR10022201[2]					0.703155 ± 9		18.3481 ± 26	15.5069 ± 25	38.3602 ± 77
RD1909-06 g[2]	Seg. 5	14.48	66.23	2936	0.703526 ± 5	0.512945 ± 9	18.7558 ± 14	15.6040 ± 13	38.9977 ± 42
RD1909-06 g[2]$							18.7544 ± 10	15.6012 ± 10	38.9961 ± 31
RD1909-06 g[2]$							18.7647 ± 10	15.6122 ± 10	39.0216 ± 30
RD1909-18 g[2]	Seg. 5	14.48	66.23	2,936	0.703526 ± 10	0.512936 ± 11	18.7513 ± 28	15.5989 ± 26	38.9848 ± 81
IR10022101*	Seg. 5	14.58	66.27	3,289	0.703378 ± 11	0.512974 ± 4			
IR10022101[2]					0.703403 ± 8	0.512987 ± 15	18.5898 ± 28	15.5686 ± 26	38.7405 ± 82
RD1908-02 g[2]	Seg. 5	14.65	66.33	3,360	0.703324 ± 9		18.5664 ± 17	15.5535 ± 16	38.7143 ± 50
RD1908-03 g[2]	Seg. 5	14.65	66.33	3,360	0.703340 ± 6		18.5756 ± 25	15.5629 ± 23	38.7435 ± 73
RD1908-03 g[2]$							18.5799 ± 8	15.5645 ± 8	38.7483 ± 24
RD1908-03 g[2]$							18.5804 ± 12	15.5635 ± 11	38.7482 ± 35
IR11022901*	Seg. 5	14.77	66.48	3,283	0.703187 ± 7	0.513016 ± 4			
IR10021901*	Seg. 5	14.84	66.60	4,110	0.703045 ± 8	0.513039 ± 4			
IR10021901[2]					0.703069 ± 7	0.513036 ± 12	18.3742 ± 23	15.5382 ± 22	38.4259 ± 68
IR10021801*	Seg. 5	14.86	66.75	3,456	0.703012 ± 7				
IR10021801[2]					0.703018 ± 9		18.3060 ± 29	15.5119 ± 27	38.2727 ± 84
RD1907-01 g[2]	Seg. 5	14.92	66.82	3,547	0.703099 ± 7	0.513067 ± 12	18.2264 ± 20	15.4970 ± 19	38.1710 ± 60
IR10021702*	Seg. 5	14.99	66.89	3,736	0.702878 ± 8	0.513084 ± 5			
RD1906-02 g[2]	Seg. 5	15.12	66.98	3,740	0.702921 ± 9	0.513089 ± 14	18.1433 ± 36	15.4838 ± 35	38.0315 ± 107
IR100215013	Seg. 5	15.15	66.89	2,272	0.702930 ± 9	0.513104 ± 8			
IR10021202*	Seg. 5	15.26	67.13	3,625	0.702899 ± 6	0.513083 ± 4			
RD1905-01 g[2]	Seg. 5	15.35	67.20	3,607	0.702873 ± 8		18.1270 ± 25	15.4841 ± 24	37.9979 ± 75
IR10020901*	Seg. 5	15.66	67.23	3,254	0.702876 ± 6	0.513112 ± 3			
RD1904-02 g[2]	Seg. 5	15.73	67.27	3,577	0.702839 ± 9		17.9117 ± 17	15.4538 ± 17	37.7424 ± 51
IR10020701*	Seg. 5	15.91	67.32	3,768	0.702905 ± 6	0.513092 ± 4			

Table 1
Continued

Sample	Segment	Latitude (°S)	Longitude (°E)	Depth (m)	$^{87}Sr/^{86}Sr$	$^{143}Nd/^{144}Nd$	$^{206}Pb/^{204}Pb$	$^{207}Pb/^{204}Pb$	$^{208}Pb/^{204}Pb$
IR10020601*	Seg. 5	16.04	67.39	4,386	0.702891 ± 6	0.513103 ± 3			
RD1902-03 g[2]	Seg. 6	16.90	66.80	3,896	0.703067 ± 5		18.1625 ± 24	15.4920 ± 23	38.1096 ± 72

Note. *, ² and ³ denote samples analysed at KBSI, KOPRI and SEDISOR, respectively. ²$ are for duplicate dissolution and Pb isotopes measurement at KOPRI. All the samples were leached in HCL before being analyzed at KBSI and KOPRI. However, no prior HCl leaching was conducted on samples analyzed at SEDISOR (see Section 4.2.).

(France) using a TIMS (a Thermo Finnigan, TRITON). Sr, Nd, and Pb isotopes of 18 samples were determined by using a TIMS (a Thermo Finnigan, TRITON) at the Korean Polar Research Institute (KOPRI). The laboratory and analytical procedures at KOPRI, KBSI, and SEDISOR for measuring isotopic compositions are described in the Text S1, S2, and S3 in Supporting Information S1, respectively.

Duplicate analyses were carried out to check possible inter-laboratory differences or possible inconsistencies between the solicited laboratories. The samples RD1908-03g and RD1909-06g have been triplicated with a complete new dissolution at KOPRI, and the values generally show good consistencies (see Table 1). One duplicate of the sample RD1909-06g shows ratios with a noticeable difference, probably due to some undefined analytical error. The other duplicate of the sample RD1909-06g analyzed at the same time does not show these differences, which demonstrates that the Pb isotope data presented in this study are reproducible. Most of the replicated isotope ratio measurements between KBSI and KOPRI do not show systematic variations. The differences outside of the uncertainties observed between duplicates of the sample IR10022301 are likely due to intrinsic heterogeneities inside the samples and neither discredit the data presented nor change the conclusion of this study. Moreover, different samples (IR10022101, IR10021901, and IR10022401) previously analyzed by Kim et al. (2017), were duplicated to verify the consistency of our analysis. The results obtained at KBSI and KOPRI show good agreement with the previous data from Kim et al. (2017), which were measured at the National Oceanography Center in the UK.

For the isotope analysis performed at KOPRI, the replicate measurements of the NBS987 and JNdi-1 standards yielded $^{87}Sr/^{86}Sr$ of 0.710264 ± 10 (2σ, n = 15) and $^{143}Nd/^{144}Nd$ of 0.512113 ± 10 (2σ, n = 15). For the Pb isotopic ratios, the replicate analyses of the NBS981 standard yielded mean values of 16.9404 ± 14 (2σ, n = 15) for $^{206}Pb/^{204}Pb$, of 15.4978 ± 20 (2σ, n = 15) for $^{207}Pb/^{204}Pb$ and of 36.7202 ± 56 (2σ, n = 15) for $^{208}Pb/^{204}Pb$. During the triplicate Pb isotopic analysis at KOPRI of the samples RD1908-03g and RD1909-06g, the mean values of the replicate measurements of the NBS981 standard were 16.9425 ± 12 (2σ, n = 7) for $^{206}Pb/^{204}Pb$, of 15.4996 ± 10 (2σ, n = 7) for $^{207}Pb/^{204}Pb$, and 36.7266 ± 22 (2σ, n = 7) for $^{208}Pb/^{204}Pb$. The total procedural blank at KOPRI for Sr, Nd, and Pb was less than 30, 20, and 50 pg, respectively. At SEDISOR, the total Sr and Nd procedural blanks were <150 pg and <70 pg, respectively, and the analysis of the NBS987 and JNdi-1 standard materials yielded the mean value of 0.710258 ± 6 (n = 2) for $^{87}Sr/^{86}Sr$ and value of 0.512111 ± 8 (n = 1) for $^{143}Nd/^{144}Nd$, respectively. The total procedural blanks for Sr and Nd were <0.1 ng at KBSI. The mean values of the repeated analyses of the NBS987 and JNdi-1 standard materials at KBSI were 0.710259 ± 9 (2σ, n = 10) for $^{87}Sr/^{86}Sr$ and 0.512120 ± 11 (2σ, n = 10) for $^{143}Nd/^{144}Nd$.

4. Results

4.1. Major and Trace Elements

Major and trace element compositions of the 25 submarine volcanic rock samples from segments 5 and 6 from 2019 R/V ISABU expedition are summarized in the Table S1 in Supporting Information S1. They range from 6.0 to 8.1 weight (wt.)% in MgO and from 50.4 to 52.2 wt.% in SiO_2. Except for CaO and Al_2O_3, which show a positive correlation, the other major elements generally display a negative correlation with MgO (Figure S1 in Supporting Information S1 presents the major element oxides vs. MgO diagrams). Na_8, the Na_2O content calculated at 8% MgO (following Klein & Langmuir, 1987, Figure S2 in Supporting Information S1), in the samples along segment 5 is 2.62 on average and does not display any systematic variations correlated with the bathymetry. Figure 2 shows the primitive mantle-normalized trace element patterns of basaltic glasses from segment 5. The result shows a large range of compositional variations from the depleted CIR MORB to E-MORB. The E-MORB

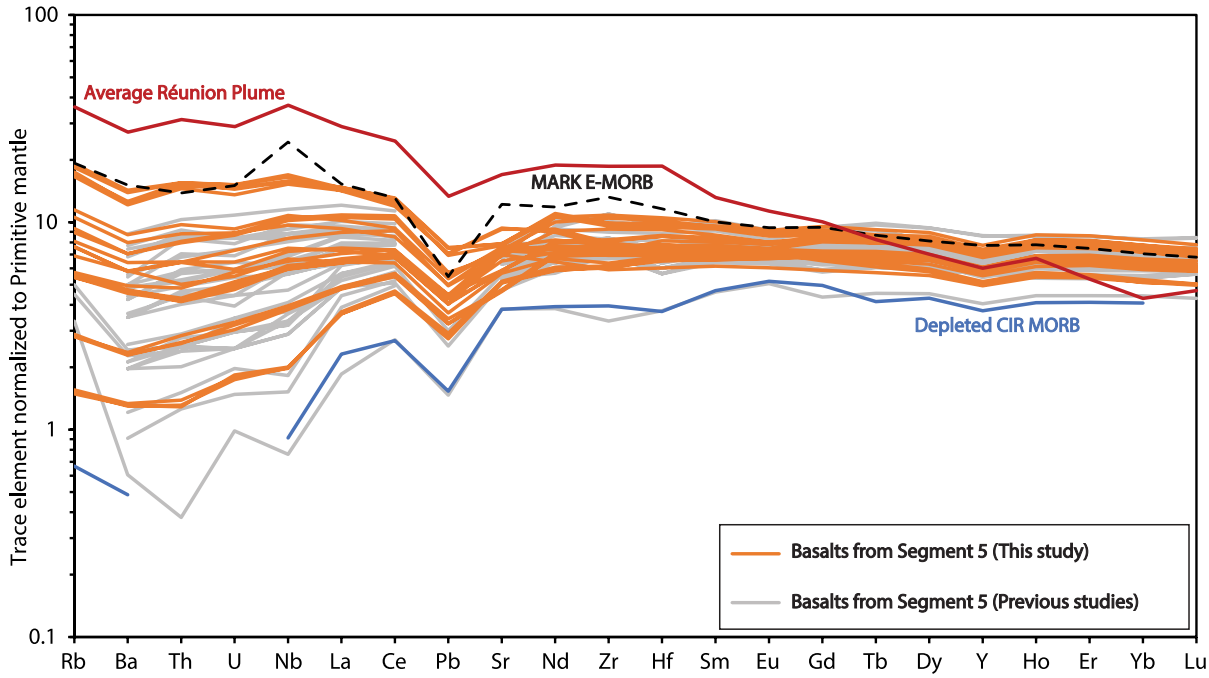

Figure 2. Trace element normalized to primitive mantle (McDonough & Sun, 1995) of basaltic glasses from segment 5. The samples from this study are shown by orange lines and by gray lines for the samples from previous studies (from PetDB database, http://www.earthchem.org/petdb). The samples from segment 5 show large compositional variations from depleted Mid-ocean ridge basalts (MORB) to enriched MORB. The averaged values of the Réunion Plume (RP) were calculated from the compositions of lavas with MgO >8 wt.% from the Mauritius-Réunion array defined by Nauret et al. (2019). The depleted Central Indian Ridge (CIR) MORB corresponds to the sample RC14 from Murton et al. (2005) and the MARK E-MORB pattern is represented by the sample All129-7 RC17A of Donnelly et al. (2004). The average RP, the MARK E-MORB and the depleted CIR MORB composition pattern are shown for comparison.

samples are more enriched in incompatible trace elements with $(La/Sm)_N > 1$ (La/Sm normalized to primitive mantle), which can be considered as a trace element proxy for mantle fertility/enrichment (Schilling, 1985; Schilling et al., 1982).

The latitudinal variations in $(La/Sm)_N$ (Figure 3) highlight substantial differences between segment 4 and the enriched segments 5 and 6. Basalts from segment 4 have N-MORB signatures with $(La/Sm)_N$ ranging from 0.65 to 1.07, whereas basalts from segment 5 show more significant latitudinal variations from south to north with $(La/Sm)_N$ ranging from 0.40 to 1.95 (Figures 3 and 4). Although less pronounced, the south-north trend is also visible along segment 6 (Figure 3). It is worth noting that the peaks of enrichment of segments 5 and 6 are located in the northern part of the segments, more precisely in the middle of segment 5-1 at 14.48°S for segment 5 (Figures 3 and 4). Different from what has been described in previous studies (Kim et al., 2017; Machida et al., 2014), our new trace element data show that some E-MORB from segment 5 are more enriched than those from segment 6, with a new maximum value in $(La/Sm)_N$ of 1.95 (sample RD1909-18g at 14.48°S).

In addition, our new samples from segments 5 and 6 present uniform Ce/Pb (~17–21) and Nb/U (~35–41) (Figure 3). The variations in these trace element ratios are of the same order of magnitude as previously reported for samples from segments 5 and 6 (and those encountered along the Rodrigues segment, south of MCFZ (Füri et al., 2011; Kim et al., 2017; Machida et al., 2014; Murton et al., 2005; Nauret et al., 2006). Overall, segment 6 shows higher variability in Ce/Pb with ratios from ~15 to 28 compared to segment 5 (Ce/Pb = 17 to 23). Two samples along segment 6 show anomalously high Nb/U (>80) ratios, probably due to loss of U (Figure 3). The samples from segments 5 and 6 have Ce/Pb and Nb/U ratios that fall within or slightly below the range for N-MORB and OIB, and no clear correlations between Nb/U, Ce/Pb, and $(La/Sm)_N$ ratios are observed (Figure 3). However, an inverse correlation between Nd/Pb and $(La/Sm)_N$ is observed along segment 5 with Nd/Pb ratios from ~10.55 to 21.7 (Figure 3). These low Nd/Pb values, especially around 14.48°S, are below the range of the global MORB and are similar to those of E-MORB along segment 6 and the Rodrigues segment (Figure 3e).

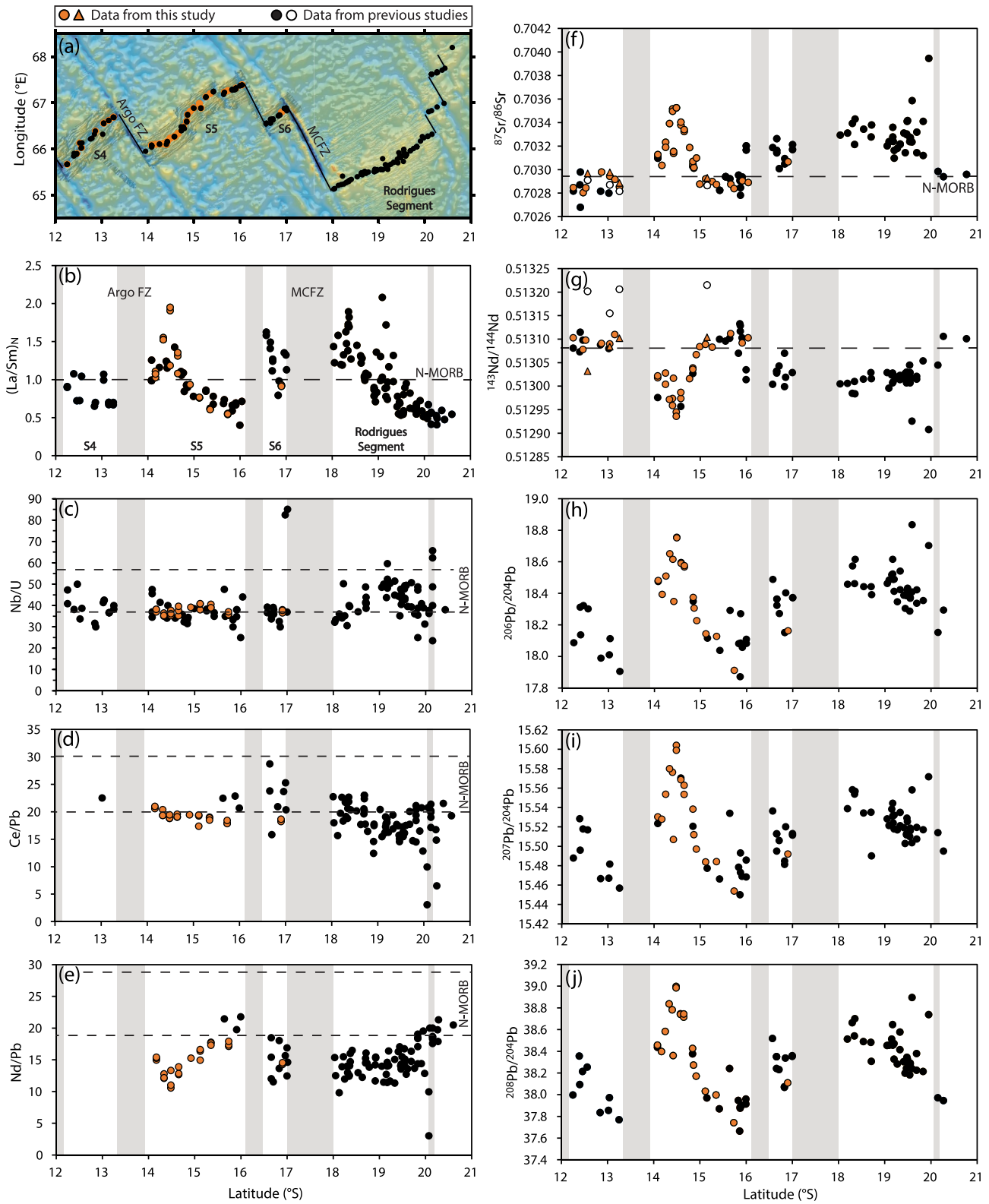

Figure 3.

4.2. Isotopic Compositions and Correlations

The 35 new Sr, Nd, and Pb isotopic analyses are compiled in Table 1 and Figures 3 and 5. It should be clarified the discrepancies between data from the previous study of Kim et al. (2017) and their duplicate presented in this study before discussion and interpretation of the isotopic variations along the CIR. Because the Sr isotopes data of the samples IR090301, IR10022701, IR10022901 and IR10021501 (white dots in Figures 3f and 3g) from segments 4 and 5 show anomalously high values given their high Nd isotopes data, Kim et al. (2017) suggested that these anomalies could be due to seawater alteration or isotopic heterogeneity in the CIR MORB mantle source. Therefore, the volcanic glasses of these four duplicate samples from segment 4 were meticulously hand-picked under a binocular microscope to avoid any possible traces of alteration as much as possible and re-analyzed without prior HCl leaching in order to confirm any possible isotopic heterogeneity or seawater alteration. The new data (orange triangles in Figures 3f and 3g) show slightly higher $^{87}Sr/^{86}Sr$ than reported by Kim et al. (2017), which can be ascribed to seawater alteration. However, the new $^{143}Nd/^{144}Nd$ isotope ratios show different signatures with substantially lower ratios within the range of other CIR N-MORB in the area (orange triangles in Figures 3f and 3g). Such differences in Nd isotope data cannot be explained by any isotopic heterogeneity or seawater alteration. Therefore, it is likely that the differences between the data are resulted from an undefined analytical artifact during the analysis of the four samples from Kim et al. (2017) and they will not be discussed in this study.

The new Sr, Nd, and Pb isotope data show that samples from segments 4, 5, and 6 range between depleted and enriched CIR MORB values (Figure 3). The most E-MORB of the studied area is sample RD1909-06g from middle of segment 5-1 ($^{87}Sr/^{86}Sr = 0.703526 \pm 5$, $^{143}Nd/^{144}Nd = 0.512945 \pm 9$, $^{206}Pb/^{204}Pb = 18.7558 \pm 14$, $^{207}Pb/^{204}Pb = 15.6040 \pm 13$; $^{208}Pb/^{204}Pb = 38.9977 \pm 42$). In contrast, MORB from segments 4, 5-2, and 5-3 fall in the range of CIR N-MORB and do not show any significant enrichment (Figures 3 and 4). The single new analysis along segment 6 shows a depleted isotopic signature resembling those previously reported for this segment at a given latitude. The new analyses along segment 5 allow us to constrain the distribution of E-MORB in the northern part of segment 5, indicating an enriched mantle present in the melting regime, as suggested by Kim et al. (2017).

The latitudinal enrichment variations observed in $(La/Sm)_N$ correlate with those of the Sr, Nd, and Pb isotopes (Figures 3 and 6a), although the Pb isotopes show more significant variability than others. Samples from segments 5 and 6 plot between a depleted MORB and the RP (Figure 6a). The most enriched portion lies in the northern part of segment 5 in the center of segment 5-1, and exhibits a signature with more radiogenic Sr and Pb isotope ratios than that of the Rodrigues segment (Figures 3–5). In the $(La/Sm)_N$ versus $^{206}Pb/^{204}Pb$ space (Figure 6a), it is noteworthy that segment 5 represents all the ranges of MORB signatures shown along the CIR from D-MORB to E-MORB with signatures identical to the RP array, thus intersecting segment 6 and the Rodrigues segment. The radiogenic Sr isotopic signature along segments 5 and 6 shows no correlation with Ce/Pb ratios. However, segments 5 and 6 samples plot mostly between a CIR D-MORB and the RP components in the $^{87}Sr/^{86}Sr$ versus Nb/U space (Figure 6). The same correlation is observed between $^{87}Sr/^{86}Sr$ and Nd/Pb ratios for the samples from segment 5. The samples with high $^{87}Sr/^{86}Sr$ have low Nd/Pb and overlap the signature of segment 6 and the Rodrigues segment, producing a trend pointing to the RP array (Figure 6b).

According to the Sr and Nd isotopic covariation diagrams (Figure 5), the samples from segment 5 follow a curvilinear trend between the depleted CIR mantle and the most enriched component represented by RD1909-06g and RD1909-18g samples in this study. This trend is more clearly shown in $^{207}Pb/^{204}Pb$ and $^{208}Pb/^{204}Pb$ versus $^{206}Pb/^{204}Pb$ covariation diagrams, which exhibit most of the samples plotting along regression lines

Figure 3. Latitudinal variations along the ridge axis of the Central Indian Ridge segments between 12° and 21°S in chemical compositions of chondrite normalized La/Sm ratios $(La/Sm)_N$, Nb/U, Ce/Pb, Nd/Pb (only glasses), and Sr, Nd and Pb isotopes of submarine basalt (whole rocks and glasses). The locations of the transform fault/fracture zone are highlighted by the gray area. The orange dots represent the data from this study. The black dots are from previous studies downloaded from the PetDB database (www.earthchem.org/petdb). The orange triangles are duplicate analyses of samples from Kim et al. (2017) showing anomalous $^{143}Nd/^{144}Nd$ (white dots). These duplicates were conducted without prior HCl leaching (see text for further information). The horizontal dashed lines and boxes indicate the average values of Mid-ocean ridge basalts (MORB) with $(La/Sm)_N = 1$ (White & Klein, 2014), Nb/U = 47 ± 10 and Ce/Pb ~ 25 ± 5 (Hofmann et al., 1986) and Nd/Pb = 24 ± 5 (Rehkamper & Hofmann, 1997). The new analysis confirm that segment 4 does not show any significant enrichment compared to the southern segment. The new samples from segment 6 do not provide new information leading to reconsider the fossil Réunion mantle component as an enriched source proposed by Kim et al. (2017). On the other hand, we note that the latitudinal variations in $(La/Sm)_N$, Nd/Pb, and isotopic compositions along the segment 5 axis are correlated, while the Ce/Pb and Nb/U ratios do not show significant variations. Also, MORB from the northern segment portion are more radiogenic (especially in lead isotopes) than those of segment 6 and the Rodrigues segment, which suggests a different enriched source. The portion of the Rodrigues segment between 19° and 20°S shows an enrichment linked to the influence of the Réunion Plume flow (Füri et al., 2011; Nauret et al., 2006).

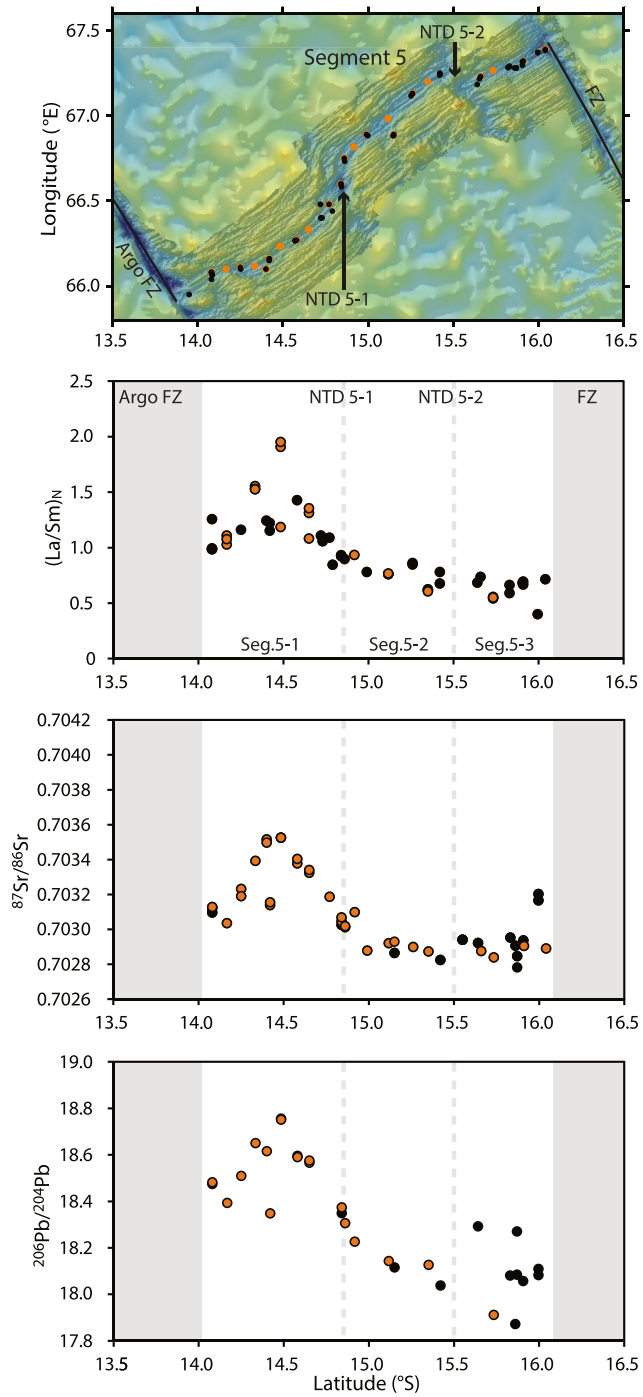

Figure 4. Latitudinal variations along the ridge axis of chondrite normalized La/Sm ratios ($(La/Sm)_N$), strontium isotopes ratios ($^{87}Sr/^{86}Sr$), and lead isotopes ratios ($^{206}Pb/^{204}Pb$) of submarine basalt from segment 5 (14° to 16.2°S). The orange dots represent the data from this study. The black dots are from previous studies downloaded from the PetDB database (www.earthchem.org/petdb). The location of the transform fault/fracture zone (FZ) and the non-transform discontinuities (NTD), identified by Pak et al. (2017), are highlighted by the gray area, and the vertical gray dashed line, respectively. We note that the enrichment characterized by high $(La/Sm)_N$, $^{87}Sr/^{86}Sr$, and $^{206}Pb/^{204}Pb$ along the segment 5 is compartmentalized between the Argo FZ and the NTD 5-1, along segment 5-1 (Seg. 5-1). The significant change in the Mid-ocean ridge basalts composition between the enriched and depleted portion across the NTD 5-1 indicate that this ridge discontinuity is likely related to the compositional change of the underlying mantle.

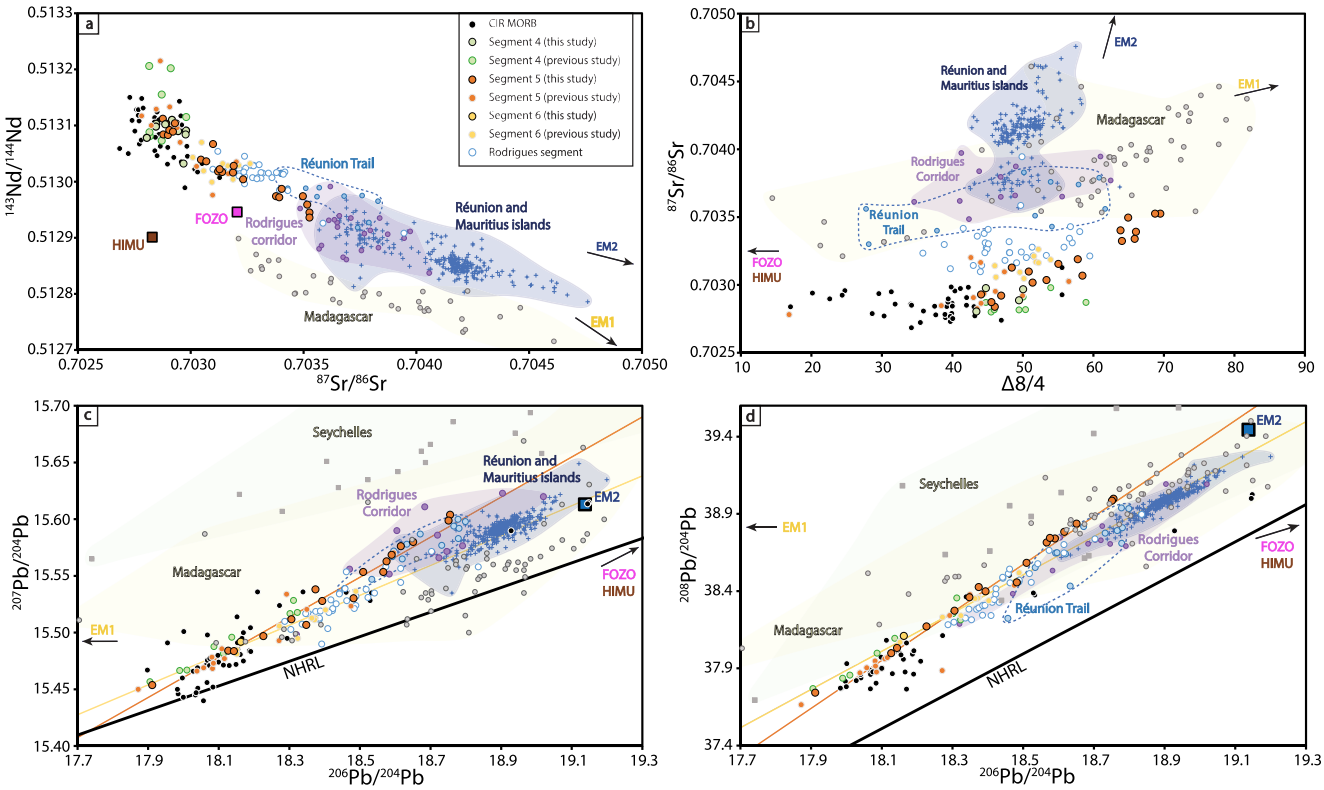

Figure 5. (a) $^{143}Nd/^{144}Nd$ versus $^{87}Sr/^{86}Sr$, (b) $^{87}Sr/^{86}Sr$ versus Δ8/4, (c) $^{207}Pb/^{204}Pb$ versus $^{206}Pb/^{204}Pb$, (d) $^{208}Pb/^{204}Pb$ versus $^{206}Pb/^{204}Pb$ covariation diagrams. Δ8/4 corresponds to the vertical deviation in $^{208}Pb/^{204}Pb$ relative to the Northern Hemisphere Reference lines (Hart, 1984). Data from our new analysis are compared with data from previous studies. The data from previous studies are downloaded from the PetDB database (www.earthchem.org/petdb). The Réunion and Mauritius islands fields correspond to the literature data compilation downloaded from the GEOROC database (DIGIS Team, 2022a, 2022b) and filtered following the method made to exclude data with large uncertainties described in Nauret et al. (2019). The data from Smietana (2011) have also been included. Réunion trail array is determined by data from White et al. (1990) (ODP Legs 115 (holes 706, 707, and 715) and industry wells (SM-1)). The Rodrigues Corridor array is defined by samples from the Rodrigues ridge and island, the Three Magi ridge, and Gasitao ridge (Baxter et al., 1985; Füri et al., 2011; Machida et al., 2014; Mellor, 1998; Nauret et al., 2006). The Seychelles field is defined by the Seychelles granitoids from Weis and Deutsch (1984) and the Madagascar field corresponds to the Cenozoic/Quaternary magmatic rocks from Madagascar (precompiled file downloaded via the GEOROC database; DIGIS Team, 2022a, 2022b). EM2 averaged isotopic composition and the EM1, FOZO and HIMU direction are from Jackson and Dasgupta (2008). The majority of enriched basalts from segment 6 and the Rodrigues segment can still be explained by a mixing between the depleted Central Indian Ridge Mid-ocean ridge basalts and a fossil Réunion component represented by the linear regression crossing the Réunion and Mauritius islands array. The refined enrichment trend observed in segment 5 is different from those of basalts from segments 6 and 7. A discrete enriched source distinct from the known Réunion Plume component is necessary to explain the enrichment along segment 5. Regression line equations for segment 5 are: $^{207}Pb/^{204}Pb = 0.176*(^{206}Pb/^{204}Pb) + 12.28$ ($R^2 = 0.958$) and $^{208}Pb/^{204}Pb = 1.55*(^{206}Pb/^{204}Pb) + 9.84$ ($R^2 = 0.965$). Regression line equations for segment 6 are: $^{207}Pb/^{204}Pb = 0.136*(^{206}Pb/^{204}Pb) + 13.00$ ($R^2 = 0.891$) and $^{208}Pb/^{204}Pb = 1.24*(^{206}Pb/^{204}Pb) + 15.60$ ($R^2 = 0.968$).

(Figures 5c and 5d) with high correlation coefficients ($R^2 > 0.95$). This trend is also visible in the covariation diagrams of $^{87}Sr/^{86}Sr$ versus Δ8/4 (Figure 5b; Δ8/4 being the vertical deviation in $^{208}Pb/^{204}Pb$ relative to the Northern Hemisphere Reference Line; Hart, 1984). The samples from segment 6 show less enriched isotopic values than those from segment 5. As presented by Kim et al. (2017), segment 6 shows a geochemical signature similar to that of the northern portion of the Rodrigues segment, and our newly obtained sample does not change the trend defined by the samples of this segment in the Sr, Nd, and Pb isotopes spaces (Figures 5 and 7).

5. Discussion

5.1. Latitudinal Variations in MORB Geochemistry and Ridge Segmentation

The absence of correlations between $(La/Sm)_N$ and Na_8 (not shown), and bathymetry suggests that the effect of partial melting degree on MORB geochemistry is limited in segments 5 and 6 as suggested by Kim et al. (2017). Furthermore, the correlation between incompatible trace element ratios such as $(La/Sm)_N$ and Sr-Nd-Pb isotope ratios suggests that MORB enrichment is due to mantle source enrichment (Figures 3, 4, and 6a).

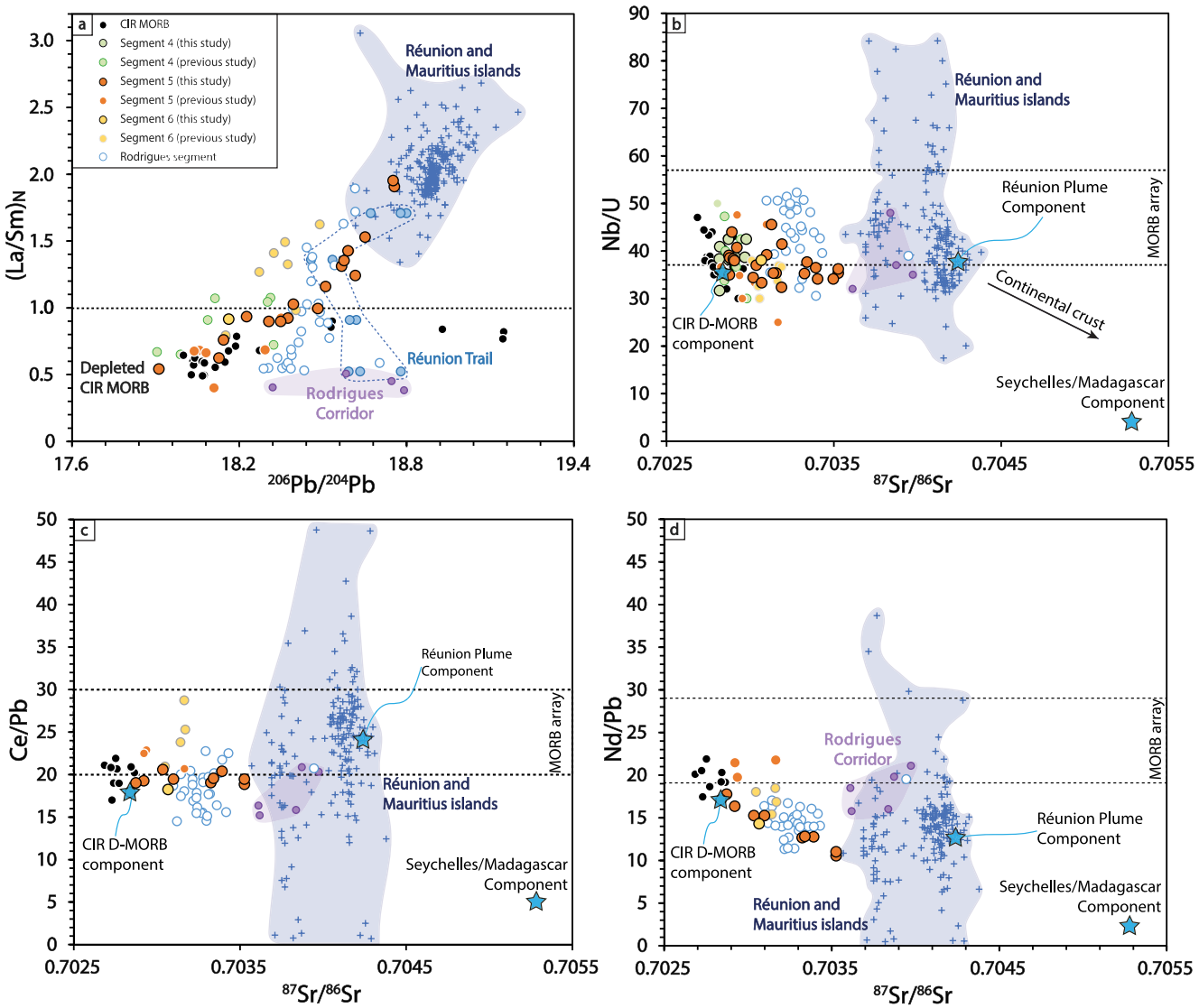

Figure 6. (a) $(La/Sm)_N$ versus $^{206}Pb/^{204}Pb$ and (b) Nb/U, (c) Ce/Pb and (d) Nd/Pb versus $^{87}Sr/^{86}Sr$ for the Central Indian Mid-ocean ridge basalts (MORB) samples (glasses). The correlation trend of $(La/Sm)_N$ ratio with $^{206}Pb/^{204}Pb$ in the direction of the Réunion Plume (RP) is visible for the MORB from segments 5 (orange dots), 6 (yellow dots) and the Rodrigues segment (blue and white dots). A correlation trend is observable in the Nd/Pb versus $^{87}Sr/^{86}Sr$ diagram for MORB from segment 5, but it is not the case in the Ce/Pb or Nb/U versus $^{87}Sr/^{86}Sr$ diagrams. However, MORB samples from segments 5, 6 and the Rodrigues segment plot in the direction of the Réunion and Mauritius plume array in these diagrams. Data from our new analysis are compared with data from previous studies that are downloaded from the PetDB database (www.earthchem.org/petdb). The Réunion and Mauritius islands field is defined from the GEOROC database (https://georoc.eu/; DIGIS Team, 2022a, 2022b) and filtered following the method made to exclude data with large uncertainties described in Nauret et al. (2019). The data from Smietana (2011) have also been included. The Réunion trail array is determined by data from White et al. (1990) (ODP Legs 115 (holes 706, 707 and 715) and industry wells (SM-1)). The Rodrigues Corridor array is defined by samples from the Rodrigues ridge and island, the Three Magi ridge, and Gasitao ridge (Baxter et al., 1985; Füri et al., 2011; Machida et al., 2014; Mellor, 1998; Nauret et al., 2006). The MORB arrays (dashed boxes) are reference values from Hofmann (2007) and Rehkamper and Hofmann (1997). The "pure" RP component is represented by sample MP 24 from Mauritius (Moore et al., 2011) with $^{87}Sr/^{86}Sr = 0.70424$, $^{206}Pb/^{204}Pb = 19.1997$ and [Nb] = 32.1 ppm [U] = 0.85 ppm [Ce] = 63.60 ppm [Pb] = 2.64 ppm (3 ppm in mixing model) [Nd] = 33.5 ppm (15 ppm in mixing model). The isotopic signature of the Seychelles/Madagascar component is from the trachytic sample "M814" from Madagascar ($^{87}Sr/^{86}Sr = 0.70528$; Cucciniello et al., 2017) and the granitic sample "9.71" from Seychelles ($^{206}Pb/^{204}Pb = 18.159$; Weis & Deutsch, 1984). Its trace element contents ([Nb] = 9.82 ppm [U] = 2.40 ppm [Ce] = 80.46 ppm [Pb] = 16 ppm [Nd] = 38 ppm) correspond to averaged values of Proterozoic plutonic/magmatic rocks from the literature data for Madagascar and Seychelles Islands (Ashwal et al., 2002; Bybee et al., 2010; Tucker et al., 1999) and downloaded from the GEOROC database (https://georoc.eu/). The depleted Central Indian Ridge MORB component is represented by the unradiogenic MORB sample RD1904-02g (this study) from segment 5 with $^{87}Sr/^{86}Sr = 0.702839$, $^{206}Pb/^{204}Pb = 17.9117$ and [Nb] = 1.32 ppm [U] = 0.04 ppm [Ce] = 7.65 ppm [Pb] = 0.43 ppm [Nd] = 7.3 ppm.

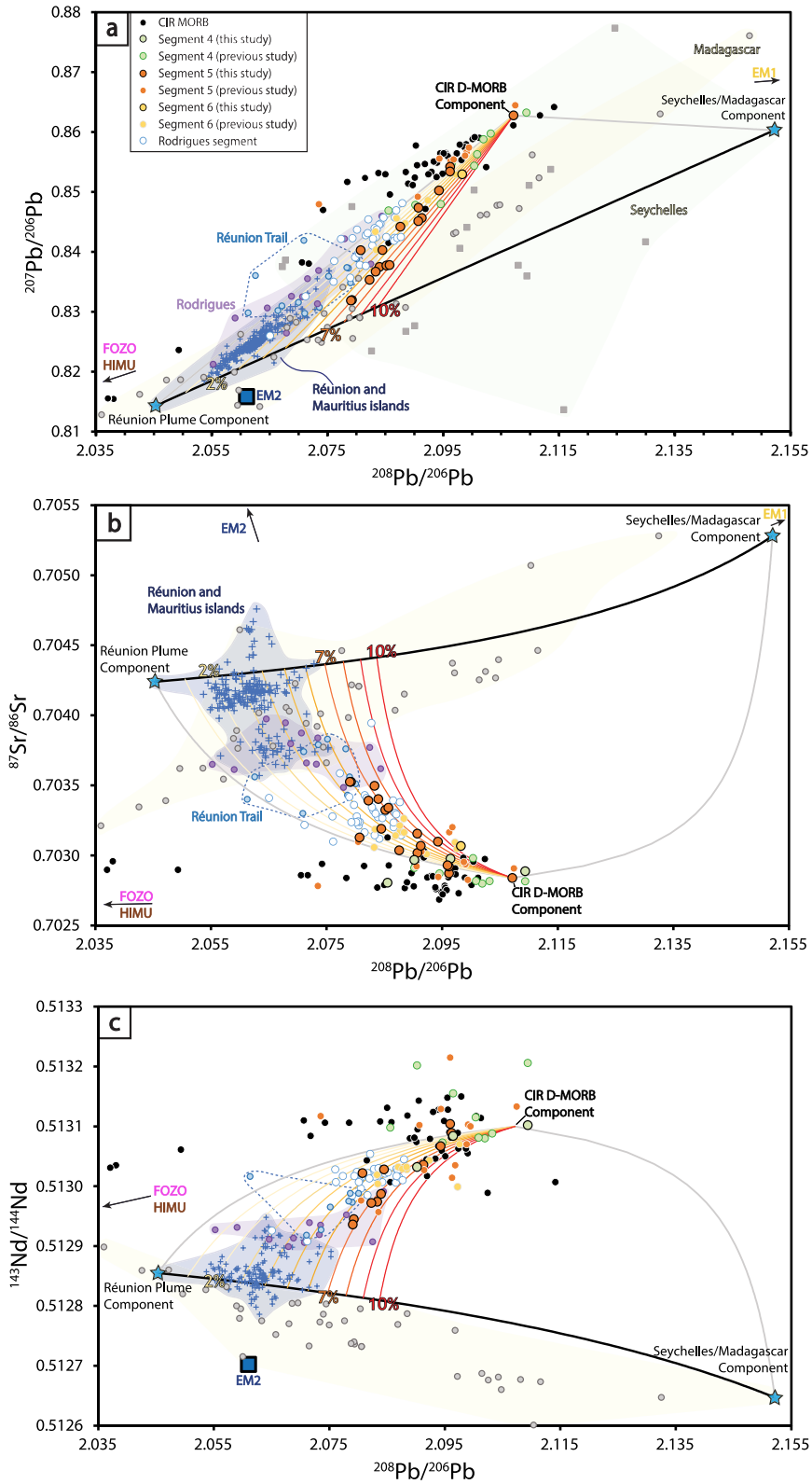

Figure 7.

The latitudinal variations in MORB chemical composition show that segment 4 is not enriched, unlike segments 5 and 6 (Figure 3). A sharp change in MORB composition is observable across the Argo fault/fracture zone (FZ) that separates segment 4 and the enriched segment 5. Indeed, the MORB samples from segment 5 are enriched in its northern part, along segment 5-1, whereas its southern section (segments 5-2 and 5-3) shows N-MORB-like geochemical signatures (Figure 4).

Moreover, the transitional change in isotopic and incompatible trace element signature along segment 5 coincides with the location of the NTD 5-1 (14.85°S, Figures 1 and 4). NTDs are commonly related to the magmatic segmentation and variations in the magmatic budget along the ridge axis with lower melt production at the NTDs regions compared to segment centers (e.g., Carbotte et al., 2016; Lin et al., 1990; Macdonald et al., 1988; Sempéré et al., 1993). Previous studies have shown that discontinuities like fracture zone/transform fault and NTDs are found bounding different chemical domains (Carbotte et al., 2016; Hamelin et al., 2010; Langmuir & Bender, 1984; Mallick et al., 2019; Meyzen et al., 2005; Smith et al., 1998). Mallick et al. (2019) showed from the geochemical variations of MORB along the East Pacific Rise that even the smallest discontinuities like devals (deviations from axial linearity, Langmuir et al., 1986) often correspond to changes in mantle source chemistry. They concluded that the changes in the mantle chemistry are a parameter that can influence discontinuities and segmentation. Moreover, it was suggested by Zheng et al. (2019) that the thermal mantle regime, a lithospheric plumbing system affecting the magma distribution and the location and nature of fertile heterogeneity in the underlying asthenosphere, are among primary factors controlling the development and propagation of NTDs. The notable change in geochemistry from a more fertile and enriched mantle under the segment 5-1 to a more depleted mantle under the segment 5-2 (Figures 3 and 4) may, therefore, be associated with the presence and location of the physical ridge segmentation represented by the NTD 5-1.

The compartmentalization of the enrichment between the Argo FZ and NTD 5-1 and the small size (∼100 km) of this enriched portion suggest the presence of small-scale and locally enriched mantle heterogeneities beneath segment 5.

5.2. Origin of the MORB Enrichment Along the Segments 5 and 6 (CIR From 14° to 17°S)

In the covariation diagram between Nd and Sr isotope ratios (Figure 5a), the MORB samples from segments 5 and 6 appear to form a mixing trend between depleted CIR MORB and the RP array defined by lavas from the Rodrigues corridor, the Réunion Trail array (White et al., 1990) and the Réunion and Mauritius islands. Data from Smietana (2011) were also incorporated into the database, which was then filtered to exclude the data with large uncertainties, as described in Nauret et al. (2019). The Rodrigues corridor array is defined by samples from the Rodrigues ridge and island, the Three Magi ridge and Gasitao ridge (Baxter et al., 1985; Füri et al., 2011; Machida et al., 2014; Mellor, 1998; Nauret et al., 2006). These structures have been described to be formed during the last s due to the influence of the RP material flowing toward the Rodrigues segment (Füri et al., 2011; Mellor, 1998; Morgan, 1978; Nauret et al., 2006).

Figure 7. (a) $^{207}Pb/^{206}Pb$ versus $^{208}Pb/^{206}Pb$, (b) $^{87}Sr/^{86}Sr$ versus $^{208}Pb/^{206}Pb$ and (c) $^{143}Nd/^{144}Nd$ versus $^{208}Pb/^{206}Pb$ covariation diagrams presenting the two-step binary mixing model between a «pure» Réunion Plume (RP) component, a Seychelles/Madagascar-like continental crust component and a depleted Central Indian Ridge (CIR) Mid-ocean ridge basalts (MORB) mantle. In this model, the RP component mixes first with the continental component that is then mixed during a second step with the CIR MORB component as proposed by Nauret et al. (2019). The model parameters used for the RP component are from sample MP 24 (Moore et al., 2011) with $^{87}Sr/^{86}Sr = 0.70424$, $^{143}Nd/^{144}Nd = 0.512857$, $^{206}Pb/^{204}Pb = 19.1997$, $^{207}Pb/^{204}Pb = 15.6350$, $^{208}Pb/^{204}Pb = 39.2697$ [Sr] = 150 ppm [Nd] = 15 ppm and [Pb] = 3 ppm. The isotopic composition of the Seychelles/Madagascar-like component is $^{87}Sr/^{86}Sr = 0.70528$, $^{143}Nd/^{144}Nd = 0.512647$, $^{206}Pb/^{204}Pb = 18.159$, $^{207}Pb/^{204}Pb = 15.622$ and $^{208}Pb/^{204}Pb = 39.081$. The model compositions in [Sr] = 270 ppm [Nd] = 38 ppm and [Pb] = 16 ppm are from Nauret et al. (2019) and are averaged values of Proterozoic plutonic/magmatic rocks from the literature data for Madagascar and Seychelles Islands (Ashwal et al., 2002; Bybee et al., 2010; Tucker et al., 1999) and downloaded from the GEOROC database (https://georoc.eu/). The slightly modified compositions of the unradiogenic MORB sample RD1904-02g (this study) is chosen to represent the depleted CIR MORB mantle with $^{87}Sr/^{86}Sr = 0.702839$, $^{143}Nd/^{144}Nd = 0.51310$, $^{206}Pb/^{204}Pb = 17.9117$, $^{207}Pb/^{204}Pb = 15.4538$, $^{208}Pb/^{204}Pb = 37.7424$ and [Sr] = 75 ppm [Nd] = 7.3 ppm [Pb] = 0.43 ppm. Data from our new analysis are compared with data from previous studies. The CIR MORB data from previous studies are downloaded from the PetDB database (www.earthchem.org/petdb) and the Madagascar data correspond to a precompiled file from the GEOROC database (DIGIS Team, 2022a, 2022b), respectively. The Seychelles field is represented by the Seychelles granitoids from Weis and Deutsch (1984). The Réunion and Mauritius islands field is defined from a GEOROC precompiled file (https://georoc.eu/; DIGIS Team, 2022a, 2022b) and filtered following the method made to exclude data with large uncertainties described in Nauret et al. (2019). The data from Smietana (2011) have also been included. The Réunion trail array is determined by data from White et al. (1990) (ODP Legs 115 (holes 706, 707 and 715) and industry wells (SM-1)). The Rodrigues Corridor array is defined by samples from the Rodrigues ridge and island, the Three Magi ridge and Gasitao ridge (Baxter et al., 1985; Füri et al., 2011; Machida et al., 2014; Mellor, 1998; Nauret et al., 2006).

The presence of a fossil Réunion mantle component in the mantle beneath segments 5 and 6 was proposed by Kim et al. (2017) as a possible enriched source in order to explain the E-MORB genesis. They showed that MORB along these segments have geochemical signatures linked to the RP. However, the direct influence of the RP has been excluded because the $^{3}He/^{4}He$ (R/R_A) values of the E-MORB samples are comparable to N-MORB (<10 R_A; R_A = air $^{3}He/^{4}He$), which is significantly lower than the enriched values from the Réunion hotspot (13–14 R_A) (Burnard et al., 1994; Graham et al., 1990) or the southern portion of the Rodrigues segment which is influenced by the plume with values greater than 10 R_A (Füri et al., 2011).

Our new single MORB data from segment 6 does not change the geochemical characteristics presented by Kim et al. (2017), and its MORB enrichment can still be linked to a fossil RP component as shown by the regression line ($R^2 > 0.89$) of segment 6 crossing the RP array (Figures 5c and 5d). The trace element geochemistry and isotopic signature of MORB from this segment are similar to the signature observed along the northern portion of the Rodrigues segment, which is suggested to be influenced by a fossil RP component by Füri et al. (2011).

Although the MORB of segments 5 and 6 seemingly all plot between the depleted CIR MORB and EM2 end-members (Figures 5 and 7), the MORB from segment 5 have higher $^{208}Pb/^{204}Pb$ and $^{207}Pb/^{204}Pb$ for a given $^{206}Pb/^{204}Pb$ (Figures 5c and 5d) than those from segment 6 or the Rodrigues segment and offset from the trend toward the RP field (Figures 5 and 6; Kim et al., 2017). Moreover, the triangular shape formed by the samples from segment 5 in the $^{208}Pb/^{206}Pb$ versus $^{207}Pb/^{206}Pb$ space (Figure 7a) seems to indicate that at least three end-members are necessary to explain the MORB enrichment encountered along this segment: a depleted and two enriched end-members. One of the enriched end-members is likely to be a fossil RP component, as observed from segment 6 (Kim et al., 2017), and the other is highlighted by the most radiogenic sample (RD1909-06g) from segment 5 and characterized by higher $^{87}Sr/^{86}Sr$ and $(La/Sm)_N$, relatively lower Nb/U and Nd/Pb as well as higher $^{208}Pb/^{204}Pb$ and $^{207}Pb/^{204}Pb$ for a given $^{206}Pb/^{204}Pb$ than the RP component.

5.2.1. Contamination of the Réunion Plume by a Continental Crust Component as a Source of the MORB Enrichment Along Segment 5?

Previous studies have highlighted the small-scale radiogenic isotopic heterogeneity of the RP during the last 10 Ma, as displayed by lavas on Mauritius and Réunion islands (e.g., Bosch et al., 2008; Moore et al., 2011; Nauret et al., 2019; Paul et al., 2005; Smietana, 2011). Various scenarios were proposed to explain the heterogeneity in the Mauritius and Réunion sources, including the presence of a third component often considered to have a DUPAL flavor (Bosch et al., 2008; Dupré & Allègre, 1983) and mixed with the RP and the depleted MORB mantle. This third component model is supported by the Archean/continental zircons discovered within Mauritian trachytes. The signature of these zircons was suggested to reflect contamination of the Mauritius plume by a continental component with Seychelles/Madagascar-like compositions (Ashwal et al., 2017; Torsvik et al., 2013). Moreover, Nauret et al. (2019) show that the isotopic variations along the Mauritius-Réunion hotspot track, mostly reflected by the Réunion lavas having higher $^{207}Pb/^{204}Pb$ and $^{208}Pb/^{204}Pb$ for a given $^{206}Pb/^{204}Pb$, are due to the involvement of three components mixed in two steps. The first step is defined by incorporating Seychelles/Madagascar-like continental crust into the RP during its ascent into the asthenosphere, which will then be mixed in a second step with the depleted Indian MORB mantle.

It turns out that, except in the Pb isotopic spaces (Figures 5 and 7), the E-MORB from segment 5 have a similar signature to that of the Rodrigues segment presented as being influenced by the Réunion and fossil RP component (Füri et al., 2011; Nauret et al., 2006). The addition of a continental component to the RP is a reasonable candidate to explain the higher $^{207}Pb/^{204}Pb$ and $^{208}Pb/^{204}Pb$ for a given $^{206}Pb/^{204}Pb$ and the relatively lower Nb/U (and Nd/Pb) ratios than N-MORB observed in these E-MORB (Figures 3 and 5–7).

A two-step quantitative mixing modeling was conducted to test whether the RP component previously mixed with a Seychelles/Madagascar-like continental crust component can explain the MORB enrichment along segment 5. The three components mixing model is presented in Figure 7, following the model from Nauret et al. (2019) with slight modifications in the choice of the end-members parameters (see caption of Figure 7 for the details of the key parameters).

As suggested by Nauret et al. (2019), the sample MP 24 from Mauritius (Moore et al., 2011) was chosen to reflect the isotopic signature of the "pure" RP component since it has the most enriched isotopic signature ($^{87}Sr/^{86}Sr$ = 0.70424, $^{143}Nd/^{144}Nd$ = 0.512857, $^{206}Pb/^{204}Pb$ = 19.1997, $^{207}Pb/^{204}Pb$ = 15.6350, $^{208}Pb/^{204}Pb$ = 39.2697) and high Ni and MgO content (Ni = 189 ppm; MgO = 9.15 wt.%). Following the suggestions from Ashwal et al. (2016)

and Nauret et al. (2019), the continental component has a Seychelles/Madagascar-like continental crust signature with $^{87}Sr/^{86}Sr = 0.70528$ and $^{143}Nd/^{144}Nd = 0.512647$ from the magmatic sample M814 (Cucciniello et al., 2017) as chosen by Nauret et al. (2019). However, the model compositions use Pb isotopic ratios of a differentiated Proterozoic magmatic rock, the granitic sample 9.71 from Seychelles ($^{206}Pb/^{204}Pb = 18.159$, $^{207}Pb/^{204}Pb = 15.622$, $^{208}Pb/^{204}Pb = 39.081$; Weis & Deutsch, 1984) which is slightly different from the ratios chosen by Nauret et al. (2019) in their mixing model but still representative of a Seychelles/Madagascar-like continental crust signature. The composition of the continental components is the same as Nauret et al. (2019) and corresponds to averaged values of Proterozoic magmatic rocks from Madagascar and Seychelles Islands (Ashwal et al., 2002; Bybee et al., 2010; Tucker et al., 1999) downloaded from the GEOROC database (https://georoc.eu/). The main difference with the model from Nauret et al. (2019) is the choice of the depleted MORB mantle component. The slightly modified composition of the particularly unradiogenic MORB sample RD1904-02g from segment 5 (this study) is chosen to represent the depleted CIR MORB mantle component. It should be noted that the mixing model result is highly dependent on the model parameters. For example, it is likely that the continental crust component signature can be temporally and spatially variable, which is consistent with the large range of isotopic signatures in the Seychelles/Madagascar array (Figures 5 and 7). However, the model is still useful in terms of explaining the general geochemical trends and constraining the mantle sources of the CIR MORB.

The model results indicate that the E-MORB signatures observed along segment 5 can be explained by the RP mixed with ∼0%–8% of Seychelles/Madagascar-like continental crust, which is then added to ∼60%–100% of the depleted CIR MORB mantle (Figure 7). The proportion of the continental component in our model is comparable with that required to account for the geochemistry of Réunion and Mauritius lavas from Nauret et al. (2019). The modified parameters used in this study do not change the conclusion of Nauret et al. (2019), and our model can also explain the isotopic variations shown between the different Mauritius and La Réunion volcanoes by the incorporation of Seychelles/Madagascar-like continental crust into the RP. The incompatible trace elements and isotopic signature of MORB along segment 5 as well as the proximity of this segment with the Réunion trail, segment 6 and Rodrigues segment suggest that the MORB enrichment may be due to a RP component that has been previously contaminated by a continental component.

5.2.2. Origin of the Crustal Component

The discovery of Archean zircons contained in the Mauritian trachytes suggests the possible continental crust contamination of the RP. Because the signature and age of the zircons are similar to the Madagascar and Seychelles continental crust, these zircons were interpreted to reflect the presence of ancient continental fragments beneath Mauritius island as well as the Mascarene plateau and the Chagos-Laccadive ridges (Ashwal et al., 2017; Torsvik et al., 2013). Like the Seychelles, this remnant of continental crust would have been separated and fragmented from Madagascar and southern India during the opening of the Mascarene basin (83.5–61 Ma). If this scenario is true, those fragments could have interacted with the RP flow when it was in proximity and provided the continental crust component necessary to explain the signature of the fossil RP heterogeneities dispersed in the Indian Ocean mantle. Based on the plate reconstruction (Chatterjee et al., 2013; Torsvik et al., 2013), the continental fragments suggested to be present under the Mascarene plateau may thus have interacted 10 to 33 Ma ago with the plume resulting in the dispersion of contaminated heterogeneities in the upper mantle. It is likely that the different continental fragments show various signatures leading to diverse plume signatures depending on which fragment contaminated the RP. Nevertheless, it is difficult to confirm any relationship with a possible continental fragment under the Mascarene plateau due to little or no information about it.

Nauret et al. (2019) argue that the continental crust component inherited in the Réunion island volcanism cannot be attributed to a continental fragment beneath La Réunion island. They suggest that the crustal contamination occurred in the asthenosphere, questioning the presence of continental fragments under Mauritius (Ashwal et al., 2017; Torsvik et al., 2013). Indeed, the bathymetry, the seismic velocity structure and the magnetic fabric show that the lithosphere beneath Réunion Island is oceanic. Also, their mixing model implies that the RP is already mixed with the crustal component before interacting with the Indian MORB mantle. Based on the signature of continental zircons found in Mauritian trachytes (Ashwal et al., 2017; Torsvik et al., 2013) as well as seismic tomography and SKS splitting studies (Mazzulo et al., 2017; Scholz et al., 2018), Nauret et al. (2019) suggest that the continental crust component affecting the RP during the last 10 Ma is located beneath Madagascar. This continental component was probably recycled into the asthenosphere during the East Africa orogeny (800–650 Ma), more precisely during the West Madagascar orogeny. Although the seismic studies seem

to indicate the presence of a low-shear-velocity root beneath Madagascar that interacts with the RP (Mazzulo et al., 2017; Scholz et al., 2018), it is likely that the East Africa orogeny also provided other continental crust heterogeneities dispersed in the Indian Ocean mantle (Nauret et al., 2019). Moreover, Nauret et al. (2019) focus on lavas erupted at the Réunion and Mauritius Islands over the past 10 Ma, but the RP flow dispersed heterogeneities in the upper mantle since 65.5 Ma (Courtillot et al., 1986; Richards et al., 1989; Torsvik et al., 2013). We note that some samples from the Réunion trail with an age of 33 Ma (e.g., ODP115 site 706) (Greenough & Fryer, 1990; White et al., 1990) show an isotopic signature that seems to have a high proportion (~5%–6%) of continental component according to our mixing model (Figure 7) or the one presented by Nauret et al. (2019) suggesting that a continental component could have affected the plume even 33 Ma ago.

It is beyond the scope of this study to date the emission of the plume heterogeneity in the upper mantle or to confirm the origin of the continental component. Nevertheless, the high correlation coefficients ($R^2 > 0.95$) of the regression lines in the Pb isotopic covariations diagrams (Figures 5c and 5d) and the Principal Component Analysis (PCA; see Results in Text S4 in Supporting Information S1) conducted on segment 5 lavas presenting a cumulative variability of 99.46% (98.76% + 0.70%) for the first principal component suggest that the continental component was mixed with the RP within the asthenosphere, before interacting with the CIR MORB mantle component. We propose that the source of the continental crust signature observed in the E-MORB from segment 5 could either be located beneath Madagascar or represent another heterogeneity (e.g., beneath the Mascarene plateau) sampled by the RP in its early history when it was closer to the ridge.

5.2.3. The Geochemical Discrepancy Between E-MORB From Segments 5, 6 and the Rodrigues Segment

Our mixing model shows that E-MORB from segment 5 can be described to a fossil RP component with varying continental crust contamination. It should be noted that the presence of a continental crust component (e.g., like Seychelles/Madagascar) with higher $^{208}Pb/^{206}Pb$ at a given $^{207}Pb/^{206}Pb$ can also explain the isotopic signatures of MORB from segment 6 and the Rodrigues segment (Figure 7), which are also influenced by a fossil RP component (Füri et al., 2011; Kim et al., 2017). The PCA analysis was conducted for the combination of MORB from segments 5 and 6 as well as for segments 5, 6 and the Rodrigues segment. The results for segments 5 and 6 show cumulative variability of 99.42% (98.41% + 1.01%) for the first two principal components, whereas those for segments 5, 6 and the Rodrigues segment display cumulative variability of 99.26% (97.14% + 2.12%). Note that the variability of the first principal component increases (97.14% compared to 98.76%) when segment 5 is added to segment 6 and the Rodrigues segment, probably due to slightly different component signatures or proportions present in the MORB source. Nauret et al. (2019) suggested that the continental component is found in all the volcanic episodes of the RP since the formation of Mauritius island (10 Ma) and even before because the RP crossed the CIR at 34 Ma (Duncan, 1990; O'Neill et al., 2003; Torsvik et al., 2013), which is consistent with the isotopic variations of the Réunion trail array (see previous section; Figures 5 and 7). Therefore, we suggest that MORB from segment 6 and the Rodrigues segment could also show the enriched signatures related to the recycled component. Our mixing model suggests that different proportions of continental crust component (0%–8%) mixed with the RP component can explain the slight difference in cumulative variability and the triangular shape formed by the MORB from segments 5 and 6 and the Rodrigues segment in the different isotopic covariation diagrams (Figures 5 and 7). It appears that the proportion of the continental crust component affecting the RP mantle signature is reduced from segment 5 (up to 8%) to the Rodrigues segment (<6%) via segment 6 (Figure 7). The non-homogeneous incorporation of variable proportions of continental crust components into the RP during its ascent through the asthenosphere (Nauret et al., 2019) may lead to spatial plume heterogeneities. The heterogeneous plume dispersed in the upper mantle and then included in the melting regime of the different segments could therefore be reflected by variable MORB signature.

6. Conclusions

The new trace element and isotope data of MORB, obtained by high spatial resolution sampling of the southern segment of the middle part of the CIR (from 12° to 17°S) provide new constraints for characterizing the MORB enrichment occurring along this ridge portion, particularly along segment 5 (14°–16.2°S). The E-MORB present along segment 5 are mostly compartmentalized between the Argo TF (14°S) and NTD 5-1 (14.85°S) and show high $(La/Sm)_N$, $^{87}Sr/^{86}Sr$ and $^{206}Pb/^{204}Pb$ with values up to 1.95, 0.703526 and 18.7558 respectively. The E-MORB signature has higher $^{207}Pb/^{204}Pb$ and $^{208}Pb/^{204}Pb$ at a given $^{206}Pb/^{204}Pb$ compared to the Réunion or fossil Réunion mantle component observable just south along segment 6 (16.5°–17°S) and the Rodrigues

segment (18°–20°S) (Füri et al., 2011; Kim et al., 2017; Murton et al., 2005; Nauret et al., 2006). Despite their EM2-like signature similar to the RP, the petrogenesis of E-MORB from segment 5 can no longer be explained by the influence of a "pure" RP component only. Following the three-component mixing model of Nauret et al. (2019), we show that the recycling under the ridge of a fossil RP heterogeneity previously contaminated by a Seychelles/Madagascar-like continental crust is a consistent scenario for the enrichment along segment 5. Moreover, this model can also explain the enrichment variations encountered along segment 6 and the Rodrigues segment by variable proportions of a crustal component mixed with the plume.

Data Availability Statement

The new data set supporting the conclusions presented in this manuscript are provided in the data table and the figures herein as well as Supporting Information S1. The new trace element and isotope data of MORB presented in this study are also archived by the EarthChem Library and are findable and accessible via https://doi.org/10.26022/IEDA/112112 (Vincent et al., 2023).

Acknowledgments

This research was financially supported by the Korean Institute of Marine Science & Technology (KIMST) funded by the Ministry of Oceans and Fisheries (MOF), Korea (Fund No. 20170411). This work was also supported by funds from MOF (Fund No. 20210634) as well as the National Research Foundation of Korea (NRF) grant funded by the Ministry of Science Information and Technology (MSIT), Korea (Fund No. 2022R1A5A1085103). The ship time and related research activities of an expedition to Indian Ocean by R/V ISABU in 2019 were funded by the MOF via KIOST (Fund No. PE99799). Dr. Mi Jung Lee and the laboratory works done at KOPRI were supported by a KOPRI grant (PE22050). We sincerely acknowledge to all participating scientists and crew members of R/V ISABU, the technical staff of KOPRI as well as Seongjun Choi, Gyuchan Park and Sunghwan Lim for their help on acquiring and processing the data presented here. We would also like to thank Christophe Hémond, Guilhem Barruol, Jérôme Dyment, Marcia Maia, Anne Briais, Kyoko Okino, Hyunwoo Lee, Jihyuk Kim and Hogyum Kim for their valuable discussions and comments on this research. We also thank Philip E. Janney, Francois Nauret and an anonymous reviewer for their constructive reviews that led to significant improvements in the manuscript.

References

Amante, C., & Eakins, B. W. (2009). ETOPO1 1 arc-minute global relief model: Procedures, data sources and analysis. NOAA technical memorandum NESDIS NGDC-24. *National Geophysical Data Center, NOAA*, *10*(2009), V5C8276M. https://doi.org/10.7289/V5C8276M

Ashwal, L. D., Demaiffe, D., & Torsvik, T. H. (2002). Petrogenesis of neoproterozoic granitoids and related rocks from the Seychelles: The case for an andean-type arc origin. *Journal of Petrology*, *43*(1), 45–83. https://doi.org/10.1093/petrology/43.1.45

Ashwal, L. D., Torsvik, T., Horváth, P., Harris, C., Webb, S., Werner, S., & Corfu, F. (2016). A mantle-derived origin for Mauritian trachytes. *Journal of Petrology*, *57*(9), 1645–1676. https://doi.org/10.1093/PETROLOGY/EGW052

Ashwal, L. D., Wiedenbeck, M., & Torsvik, T. H. (2017). Archaean zircons in Miocene oceanic hotspot rocks establish ancient continental crust beneath Mauritius. *Nature Communications*, *8*(1), 1–9. https://doi.org/10.1038/ncomms14086

Barruol, G., Sigloch, K., Scholz, J.-R., Mazzullo, A., Stutzmann, E., Montagner, J.-P., et al. (2019). Large-scale flow of Indian Ocean asthenosphere driven by Réunion plume. *Nature Geoscience*, *12*(12), 1043–1049. https://doi.org/10.1038/s41561-019-0479-3

Baxter, A. N., Upton, B. G. J., & White, W. M. (1985). Petrology and geochemistry of Rodrigues Island, Indian Ocean. *Contributions to Mineralogy and Petrology*, *89*(1), 90–101. https://doi.org/10.1007/BF01177594

Bosch, D., Blichert-Toft, J., Moynier, F., Nelson, B. K., Telouk, P., Gillot, P. Y., & Albarède, F. (2008). Pb, Hf and Nd isotope compositions of the two réunion volcanoes (Indian Ocean): A tale of two small-scale mantle "blobs". *Earth and Planetary Science Letters*, *265*(3–4), 748–765. https://doi.org/10.1016/J.EPSL.2007.11.018

Burnard, P. G., Stuart, F. M., Turner, G., & Oskarsson, N. (1994). Air contamination of basaltic magmas: Implications for high 3 He/4 He mantle Ar isotopic composition. *Journal of Geophysical Research*, *99*(B9), 17709–17715. https://doi.org/10.1029/94JB01191

Bybee, G. M., Ashwal, L. D., & Wilson, A. H. (2010). New evidence for a volcanic arc on the Western margin of a rifting Rodinia from ultramafic intrusions in the Andriamena region, north-central Madagascar. *Earth and Planetary Science Letters*, *293*(1–2), 42–53. https://doi.org/10.1016/j.epsl.2010.02.017

Carbotte, S. M., Smith, D. K., Cannat, M., & Klein, E. M. (2016). Tectonic and magmatic segmentation of the global ocean ridge system: A synthesis of observations. *Geological Society—Special Publications*, *420*(1), 249–295. https://doi.org/10.1144/SP420.5

Chatterjee, S., Goswami, A., & Scotese, C. R. (2013). The longest voyage: Tectonic, magmatic, and paleoclimatic evolution of the Indian plate during its northward flight from Gondwana to Asia. *Gondwana Research*, *23*(1), 238–267. https://doi.org/10.1016/j.gr.2012.07.001

Courtillot, V., Besse, J., Vandamme, D., Montigny, R., Jaeger, J.-J., & Cappetta, H. (1986). Deccan flood basalts at the Cretaceous/Tertiary boundary? *Earth and Planetary Science Letters*, *80*(3–4), 361–374. https://doi.org/10.1016/0012-821X(86)90118-4

Cucciniello, C., Melluso, L., le Roex, A. P., Jourdan, F., Morra, V., de 'Gennaro, R., & Grifa, C. (2017). From olivine nephelinite, basanite and basalt to peralkaline trachyphonolite and comendite in the ankaratra volcanic complex, Madagascar: 40Ar/39Ar ages, phase compositions and bulk-rock geochemical and isotopic evolution. *Lithos*, *274*, 363–382. https://doi.org/10.1016/J.LITHOS.2016.12.026

DeMets, C., Gordon, R. G., & Argus, D. F. (2010). Geologically current plate motions. *Geophysical Journal International*, *181*(1), 1–80. https://doi.org/10.1111/j.1365-246X.2009.04491.x

DeMets, C., Gordon, R. G., Argus, D. F., & Stein, S. (1990). Current plate motions. *Geophysical Journal International*, *101*(2), 425–478. https://doi.org/10.1111/j.1365-246X.1990.tb06579.x

DeMets, C., Gordon, R. G., & Vogt, P. (1994). Location of the Africa-Australia-India Triple junction and motion between the Australian and Indian plates: Results from an aeromagnetic investigation of the central Indian and Carlsberg ridges. *Geophysical Journal International*, *119*(3), 893–930. https://doi.org/10.1111/j.1365-246X.1994.tb04025.x

DIGIS Team. (2022a). *2022-02-WFJZKY_MASCARENE_ISLANDS_INCL_REUNION.csv*. GEOROC Compilation: Ocean Island Groups. GRO.data, V4. https://doi.org/10.25625/WFJZKY/7DDWBS

DIGIS Team. (2022b). *2022-09- RZZ9VM_Madagascar_CENOZOIC_QUATERNARY.csv*. GEOROC Compilation: Intraplate Volcanic Rocks. GRO.data, V4. https://doi.org/10.25625/RZZ9VM/GCC9J1

Donnelly, K. E., Goldstein, S. L., Langmuir, C. H., & Spiegelman, M. (2004). Origin of enriched ocean ridge basalts and implications for mantle dynamics. *Earth and Planetary Science Letters*, *226*(3–4), 347–366. https://doi.org/10.1016/j.epsl.2004.07.019

Duncan, R. A. (1990). The volcanic record of the reunion hotspot. *Proceedings of the Scientific Results, ODP, Leg 115, Mascarene Plateau*, *115*, 3–10.

Duncan, R. A., Backman, J., & Peterson, L., & The Shipboard Scientific Party. (1989). Reunion hotspot activitity through tertiary time: Initial results from the ocean drilling program, leg 115. *Journal of Volcanology and Geothermal Research*, *36*(1–3), 193–198. https://doi.org/10.1016/0377-0273(89)90013-9

Dupré, B., & Allègre, C. J. (1983). Pb–Sr isotope variation in Indian Ocean basalts and mixing phenomena. *Nature*, *303*(5913), 142–146. https://doi.org/10.1038/303142a0

Füri, E., Hilton, D. R., Murton, B. J., Hémond, C., Dyment, J., & Day, J. M. D. (2011). Helium isotope variations between Réunion Island and the Central Indian Ridge (17°–21°S): New evidence for ridge–hot spot interaction. *Journal of Geophysical Research*, *116*(B2), B02207. https://doi.org/10.1029/2010JB007609

Gale, N. H. (1996). A new method for extracting and purifying lead from difficult matrices for isotopic analysis. *Analytica Chimica Acta*, *332*(1), 15–21. https://doi.org/10.1016/0003-2670(96)00207-3

Galer, S. J. G., & O'Nions, R. K. (1986). Magma Genesis and the mapping of chemical and isotopic variations in the mantle. *Chemical Geology*, *56*(1–2), 45–61. https://doi.org/10.1016/0009-2541(86)90109-9

Gillot, P.-Y., & Nativel, P. (1989). Eruptive history of the Piton de la Fournaise volcano, Reunion Island, Indian Ocean. *Journal of Volcanology and Geothermal Research*, *36*(1–3), 53–65. https://doi.org/10.1016/0377-0273(89)90005-X

Graham, D., Lupton, J., Albarède, F., & Condomines, M. (1990). Extreme temporal homogeneity of helium isotopes at Piton de la Fournaise, Réunion Island. *Nature*, *347*(6293), 545–548. https://doi.org/10.1038/347545a0

Greenough, J. D., & Fryer, B. J. (1990). Distribution of gold, palladium, platinum, rhodium, ruthenium, and iridium in leg 115 hotspot basalts: Implications for magmatic processes. In *Proceedings of the ocean drilling program, 115 scientific results*. Ocean Drilling Program. https://doi.org/10.2973/odp.proc.sr.115.128.1990

Hamelin, C., Dosso, L., Hanan, B., Barrat, J.-A., & Ondréas, H. (2010). Sr-Nd-Hf isotopes along the Pacific Antarctic Ridge from 41 to 53°S. *Geophysical Research Letters*, *37*(10). https://doi.org/10.1029/2010GL042979

Hart, S. R. (1984). A large-scale isotope anomaly in the Southern Hemisphere mantle. *Nature*, *309*(5971), 753–757. https://doi.org/10.1038/309753a0

Hart, S. R., Schilling, J.-G., & Powell, J. L. (1973). Basalts from Iceland and along the Reykjanes ridge: Sr Isotope geochemistry. *Nature; Physical Science*, *246*(155), 104–107. https://doi.org/10.1038/physci246104a0

Hémond, C., Hofmann, A. W., Vlastélic, I., & Nauret, F. (2006). Origin of MORB enrichment and relative trace element compatibilities along the mid-Atlantic ridge between 10° and 24°N. *Geochemistry, Geophysics, Geosystems*, *7*(12). https://doi.org/10.1029/2006GC001317

Hofmann, A. W. (1997). Mantle geochemistry: The message from oceanic volcanism. *Nature*, *385*(6613), 219–229. https://doi.org/10.1038/385219a0

Hofmann, A. W. (2007). Sampling mantle heterogeneity through oceanic basalts: Isotopes and trace elements. *Treatise on Geochemistry*, *2–9*, 1–44. https://doi.org/10.1016/B0-08-043751-6/02123-X

Hofmann, A. W., Jochum, K. P., Seufert, M., & White, W. M. (1986). Nb and Pb in oceanic basalts: New constraints on mantle evolution. *Earth and Planetary Science Letters*, *79*(1–2), 33–45. https://doi.org/10.1016/0012-821X(86)90038-5

Hofmann, A. W., & White, W. M. (1982). Mantle plumes from ancient oceanic crust. *Earth and Planetary Science Letters*, *57*(2), 421–436. https://doi.org/10.1016/0012-821X(82)90161-3

Ito, G., Lin, J., & Graham, D. (2003). Observational and theoretical studies of the dynamics of mantle plume-mid-ocean ridge interaction. *Reviews of Geophysics*, *41*(4). https://doi.org/10.1029/2002RG000117

Jackson, M. G., & Dasgupta, R. (2008). Compositions of HIMU, EM1, and EM2 from global trends between radiogenic isotopes and major elements in ocean Island basalts. *Earth and Planetary Science Letters*, *276*(1-2), 175–186. https://doi.org/10.1016/j.epsl.2008.09.023

Kim, J., Pak, S.-J., Moon, J.-W., Lee, S.-M., Oh, J., & Stuart, F. M. (2017). Mantle heterogeneity in the source region of mid-ocean ridge basalts along the northern Central Indian Ridge (8°S–17°S). *Geochemistry, Geophysics, Geosystems*, *18*(4), 1419–1434. https://doi.org/10.1002/2016GC006673

Kim, J., Park, J. W., Lee, M. J., Lee, J. I., & Kyle, P. R. (2019). Evolution of alkalic magma systems: Insight from coeval evolution of sodic and potassic fractionation lineages at the pleiades volcanic complex, Antarctica. *Journal of Petrology*, *60*(1), 117–150. https://doi.org/10.1093/petrology/egy108

Klein, E. M., & Langmuir, C. H. (1987). Global correlations of ocean ridge basalt chemistry with axial depth and crustal thickness. *Journal of Geophysical Research*, *92*(B8), 8089. https://doi.org/10.1029/JB092iB08p08089

Langmuir, C. H., Bender, J. F., & Batiza, R. (1986). Petrological and tectonic segmentation of the East Pacific rise, 5°30′-14°30′ N. *Nature*, *322*(6078), 422–429. https://doi.org/10.1038/322422a0

Langmuir, C. H., & Bender, J. F. (1984). The geochemistry of oceanic basalts in the vicinity of transform faults: Observations and implications. *Earth and Planetary Science Letters*, *69*(1), 107–127. https://doi.org/10.1016/0012-821X(84)90077-3

Lee, M. J., Lee, J. I., Kim, T. H., Lee, J., & Nagao, K. (2015). Age, geochemistry and Sr-Nd-Pb isotopic compositions of alkali volcanic rocks from Mt. Melbourne and the Western Ross Sea, Antarctica. *Geosciences Journal*, *19*(4), 681–695. https://doi.org/10.1007/s12303-015-0061-y

Lin, J., Purdy, G. M., Schouten, H., Sempere, J. C., & Zervas, C. (1990). Evidence from gravity data for focused magmatic accretion along the mid-Atlantic ridge. *Nature*, *344*(6267), 627–632. https://doi.org/10.1038/344627a0

Macdonald, K. C., Fox, P. J., Perram, L. J., Eisen, M. F., Haymon, R. M., Miller, S. P., et al. (1988). A new view of the mid-ocean ridge from the behaviour of ridge-axis discontinuities. *Nature*, *335*(6187), 217–225. https://doi.org/10.1038/335217a0

Machida, S., Orihashi, Y., Magnani, M., Neo, N., Wilson, S., Tanimizu, M., et al. (2014). Regional mantle heterogeneity regulates melt production along the Réunion hotspot-influenced Central Indian Ridge. *Geochemical Journal*, *48*(5), 433–449. https://doi.org/10.2343/geochemj.2.0320

Mahoney, J. J., Natland, J. H., White, W. M., Poreda, R., Bloomer, S. H., Fisher, R. L., & Baxter, A. N. (1989). Isotopic and geochemical provinces of the Western Indian Ocean spreading centers. *Journal of Geophysical Research*, *94*(B4), 4033–4052. https://doi.org/10.1029/JB094IB04P04033

Mallick, S., Salters, V. J. M., & Langmuir, C. H. (2019). Geochemical variability along the Northern East Pacific rise: Coincident source composition and ridge segmentation. *Geochemistry, Geophysics, Geosystems*, *20*(4), 1889–1911. https://doi.org/10.1029/2019GC008287

Mazzullo, A., Stutzmann, E., Montagner, J. P., Kiselev, S., Maurya, S., Barruol, G., & Sigloch, K. (2017). Anisotropic tomography around La réunion Island from Rayleigh waves. *Journal of Geophysical Research: Solid Earth*, *122*(11), 9132–9148. https://doi.org/10.1002/2017JB014354

McDonough, W. F., & Sun, S.-S. (1995). The composition of the Earth. *Chemical Geology*, *120*(3–4), 223–253. https://doi.org/10.1016/0009-2541(94)00140-4

McDougall, I., Upton, B. G. J., & Wadsworth, W. J. (1965). A geological reconnaissance of Rodriguez Island, Indian Ocean. *Nature*, *206*(4979), 26–27. https://doi.org/10.1038/206026a0

McKenzie, D., & Sclater, J. G. (1971). The evolution of the Indian Ocean since the late cretaceous. *Geophysical Journal International*, *24*(5), 437–528. https://doi.org/10.1111/j.1365-246X.1971.tb02190.x

Mellor, S. H. (1998). The geochemistry and petrology of the Rodrigues Ridge (Western Indian Ocean).

Meyzen, C. M., Ludden, J. N., Humler, E., Luais, B., Toplis, M. J., Mével, C., & Storey, M. (2005). New insights into the origin and distribution of the DUPAL isotope anomaly in the Indian Ocean mantle from MORB of the Southwest Indian Ridge. *Geochemistry, Geophysics, Geosystems*, *6*(11), Q11K11. https://doi.org/10.1029/2005GC000979@10.1002/(ISSN)1525-2027.SWIR1

Moore, J., White, W. M., Paul, D., Duncan, R. A., Abouchami, W., & Galer, S. J. G. (2011). Evolution of shield-building and rejuvenescent volcanism of Mauritius. *Journal of Volcanology and Geothermal Research*, *207*(1–2), 47–66. https://doi.org/10.1016/J.JVOLGEORES.2011.07.005

Morgan, W. J. (1978). Rodriguez, Darwin, Amsterdam, A second type of hotspot Island. *Journal of Geophysical Research*, *83*(B11), 5355. https://doi.org/10.1029/JB083iB11p05355

Münch, U., Blum, N., & Halbach, P. (1999). Mineralogical and geochemical features of sulfide chimneys from the MESO zone, Central Indian Ridge. *Chemical Geology*, *155*(1–2), 29–44. https://doi.org/10.1016/S0009-2541(98)00139-9

Murton, B. J., Tindle, A. G., Milton, J. A., & Sauter, D. (2005). Heterogeneity in southern Central Indian Ridge MORB: Implications for ridge-hot spot interaction. *Geochemistry, Geophysics, Geosystems*, *6*(3), Q03E20. https://doi.org/10.1029/2004GC000798

Nauret, F., Abouchami, W., Galer, S., Hofmann, A., Hemond, C., Chauvel, C., & Dyment, J. (2006). Correlated trace element-Pb isotope enrichments in Indian MORB along 18–20°S, Central Indian Ridge. *Earth and Planetary Science Letters*, *245*(1–2), 137–152. https://doi.org/10.1016/j.epsl.2006.03.015

Nauret, F., Famin, V., Vlastélic, I., & Gannoun, A. (2019). A trace of recycled continental crust in the Réunion hotspot. *Chemical Geology*, *524*, 67–76. https://doi.org/10.1016/j.chemgeo.2019.06.009

O'Neill, C., Müller, D., & Steinberger, B. (2003). Geodynamic implications of moving Indian Ocean hotspots. *Earth and Planetary Science Letters*, *215*(1–2), 151–168. https://doi.org/10.1016/S0012-821X(03)00368-6

Park, J. W., Campbell, I. H., & Eggins, S. M. (2012). Enrichment of Rh, Ru, Ir and Os in Cr spinels from oxidized magmas: Evidence from the Ambae volcano, Vanuatu. *Geochimica et Cosmochimica Acta*, *78*, 28–50. https://doi.org/10.1016/j.gca.2011.11.018

Pak, S. J., Moon, J. W., Kim, J., Chandler, M. T., Kim, H. S., Son, J., et al. (2017). Widespread tectonic extension at the Central Indian Ridge between 8°S and 18°S. *Gondwana Research*, *45*, 163–179. https://doi.org/10.1016/j.gr.2016.12.015

Paul, D., White, W. M., & Blichert-Toft, J. (2005). Geochemistry of Mauritius and the origin of rejuvenescent volcanism on oceanic island volcanoes. *Geochemistry, Geophysics, Geosystems*, *6*(6), Q06007. https://doi.org/10.1029/2004GC000883

Rehkamper, M., & Hofmann, A. W. (1997). Recycled ocean crust and sediment in Indian Ocean MORB. *Earth and Planetary Science Letters*, *147*(1–4), 93–106. https://doi.org/10.1016/S0012-821X(97)00009-5

Révillon, S., Jouet, G., Bayon, G., Rabineau, M., Dennielou, B., Hémond, C., & Berné, S. (2011). The provenance of sediments in the Gulf of Lions, Western Mediterranean Sea. *Geochemistry, Geophysics, Geosystems*, *12*(8), Q08006. https://doi.org/10.1029/2011GC003523

Richards, M. A., Duncan, R. A., & Courtillot, V. E. (1989). Flood basalts and hot-spot tracks: Plume heads and tails. *Science*, *246*(4926), 103–107. https://doi.org/10.1126/science.246.4926.103

Schilling, J. G. (1973). Iceland Mantle plume: Geochemical study of Reykjanes ridge. *Nature*, *242*(5400), 565–571. https://doi.org/10.1038/242565a0

Schilling, J. G. (1985). Upper mantle heterogeneities and dynamics. *Nature*, *314*(6006), 62–67. https://doi.org/10.1038/314062a0

Schilling, J. G., Kingsley, R. H., & Devine, J. D. (1982). Galapagos hot spot - Spreading center system 1. Spatial petrological and geochemical variations (83°W-101°W). *Journal of Geophysical Research*, *87*(B7), 5593–5610. https://doi.org/10.1029/JB087iB07p05593

Scholz, J. R., Barruol, G., Fontaine, F. R., Mazzullo, A., Montagner, J. P., Stutzmann, E., et al. (2018). SKS splitting in the Western Indian Ocean from land and seafloor seismometers: Plume, plate and ridge signatures. *Earth and Planetary Science Letters*, *498*, 169–184. https://doi.org/10.1016/J.EPSL.2018.06.033

Sempéré, J. C., Lin, J., Brown, H. S., Schouten, H., & Purdy, G. M. (1993). Segmentation and morphotectonic variations along a slow-spreading center: The mid-Atlantic ridge (24°00′ N–30°40′ N). *Marine Geophysical Researches*, *15*(3), 153–200. https://doi.org/10.1007/BF01204232

Shibata, T., & Yoshikawa, M. (2004). Precise isotope determination of trace amounts of Nd in magnesium-rich samples. *Journal of the Mass Spectrometry Society of Japan*, *52*(6), 317–324. https://doi.org/10.5702/massspec.52.317

Smietana, M. (2011). Pétrologie, géochronologie (K-Ar) et géochimie élémentaire et isotopique (Sr, Nd, Hf, Pb) de laves anciennes de la Réunion: Implications sur la construction de l'édifice volcanique. Retrieved from http://www.theses.fr/2011LARE0012/document

Smith, S. E., Casey, J. R., Bryan, W. B., Dmitriev, L., Silantyev, S., & Magakyan, R. (1998). Geochemistry of basalts from the hayes transform region of the mid-Atlantic ridge. *Journal of Geophysical Research*, *103*(B3), 5305–5329. https://doi.org/10.1029/97JB03208

Torsvik, T. H., Amundsen, H., Hartz, E. H., Corfu, F., Kusznir, N., Gaina, C., et al. (2013). A precambrian microcontinent in the Indian Ocean. *Nature Geoscience*, *6*(3), 223–227. https://doi.org/10.1038/ngeo1736

Tucker, R. D., Ashwal, L. D., Handke, M. J., Hamilton, M. A., Le Grange, M., & Rambeloson, R. A. (1999). U-Pb geochronology and isotope geochemistry of the Archean and Proterozoic rocks of north-central Madagascar. *The Journal of Geology*, *107*(2), 135–153. https://doi.org/10.1086/314337

Ulrich, M., Hémond, C., Nonnotte, P., & Jochum, K. P. (2012). OIB/seamount recycling as a possible process for E-MORB Genesis. *Geochemistry, Geophysics, Geosystems*, *13*(6). https://doi.org/10.1029/2012GC004078

Vincent, C., Park, J., Lee, S., Kim, J., Lee, M., & Révillon, S. (2023). *MORB geochemistry from the Central Indian Ridge segments between 12°S and 17°S., version 1.0*. Interdisciplinary Earth Data Alliance (IEDA). https://doi.org/10.26022/IEDA/112112

Weis, D., & Deutsch, S. (1984). Nd and Pb isotope evidence from the Seychelles granites and their xenoliths: Mantle origin with slight upper-crust interaction for alkaline anorogenic complexes. *Chemical Geology*, *46*(1), 13–35. https://doi.org/10.1016/0009-2541(84)90163-3

White, W. M., Cheatham, M. M., & Duncan, R. A. (1990). Isotope geochemistry of leg 115 basalts and inferences on the history of the réunion mantle plume. In *Proceedings of the ocean drilling program, 115 scientific results* (Vol. 115, pp. 53–61). Ocean Drilling Program. https://doi.org/10.2973/odp.proc.sr.115.131.1990

White, W. M., & Klein, E. M. (2014). Composition of the oceanic crust. In *Treatise on geochemistry* (pp. 457–496). Elsevier. https://doi.org/10.1016/B978-0-08-095975-7.00315-6

Zheng, T., Tucholke, B. E., & Lin, J. (2019). Long-term evolution of nontransform discontinuities at the mid-Atlantic ridge, 24°N–27°30′N. *Journal of Geophysical Research: Solid Earth*, *124*(10), 10023–10055. https://doi.org/10.1029/2019JB017648